

# Rain-on-snow responses to a warmer Pyrenees: a sensitivity analysis using a physically-based hydrological model

Josep Bonsoms<sup>1</sup>, Juan I. López-Moreno<sup>2</sup>, Esteban Alonso-González<sup>3</sup>, César Deschamps-Berger<sup>2</sup>, Marc Oliva<sup>1</sup>

<sup>1</sup> Department of Geography, Universitat de Barcelona, Barcelona, Spain

<sup>2</sup> Instituto Pirenaico de Ecología (IPE-CSIC), Campus de Aula Dei, Zaragoza, Spain

<sup>3</sup> Centre d'Etudes Spatiales de la Biosphère (CESBIO), Université de Toulouse, CNES/CNRS/IRD/UPS, Toulouse, France.

Corresponding author: Juan I. López-Moreno (nlopez@ipe.csic.es)

**Abstract.** Climate warming is changing the magnitude, timing, and spatial patterns of mountain snowpacks. A warmer atmosphere may also lead to precipitation phase shifts, with decreased snowfall fraction (Sf). The combination of Sf and snowpack decreases directly affects the frequency and intensity of rain-on-snow (ROS) events, a common cause of flash-flood events in snow dominated regions. In this work we examine the ROS patterns and sensitivity to temperature and precipitation change in the Pyrenees modelling through a physical-based snow model forced with reanalysis climate data perturbed following 21<sup>st</sup> century climate projections for this mountain range. ROS patterns are characterized by their frequency, rainfall quantity and snow ablation. The highest ROS frequency for the baseline climate period (1980 – 2019) are found in South-West high-elevations sectors of the Pyrenees (17 days/year). Maximum ROS rainfall amount is detected in South-East mid-elevations areas (45 mm/day, autumn), whereas the highest ROS ablation is found in North-West high-elevations zones (- 10 cm/day, summer). When air temperature is increased from 1°C to 4°C with respect to the baseline climate period, ROS rainfall amount and frequency increase at a constant rate during winter and early spring for all elevation zones. For the rest of the seasons, non-linear responses of the ROS frequency and ablation to warming are found. Overall, ROS frequency decreases in the shoulders of the season across eastern low-elevated zones due to snow cover depletion. However, ROS increases in cold, high-elevated zones where long-lasting snow cover exists until late spring. Similarly, warming triggers fast ROS ablation (+ 10% per °C) during the coldest months of the season, high-elevations, and northern sectors where the deepest snow depths are found. On the contrary, small differences in ROS ablation are found for warm and marginal snowpacks. These results highlight the different ROS responses to warming across the mountain range, suggest similar ROS sensitivities in near mid-latitude zones, and will help anticipate future ROS impacts in hydrological, environmental, and socioeconomic mountain systems.

**Keywords:** Snow, Rain-on-snow, Climate warming, Snow sensitivity, Mountain snowpack, Pyrenees.

## 1 Introduction

26

27 Mountain snowpacks supply large hydrological resources to the lowlands (García-Ruiz et al., 2015; Viviroli et  
28 al., 2011), with important implications in the ecological (Wipf and Rixen, 2010), hydrological (Barnett, 2005;  
29 Immerzeel et al., 2020) and socioeconomic systems by providing hydroelectricity (Beniston et al., 2018) or  
30 guaranteeing winter tourism activities (Spandre et al., 2019). Climate warming, however, is modifying  
31 mountain snowfall patterns (IPCC, 2022), through temperature-induced precipitation changes from snowfall  
32 to rainfall (Lynn et al., 2020), leading in some cases to rain-on-snow (ROS) events in snow covered areas. The  
33 upward high-latitude temperature and precipitation trends (Bintanja and Andry, 2017) and warming in  
34 mountain regions (Pepin et al., 2022) will likely change future ROS frequency in snow-dominated areas  
35 (López-Moreno et al., 2021). To date, research has been focused on the ROS predictability (Corripio and  
36 López-Moreno, 2017), detection and validation methods through remote sensing (Bartsch et al., 2010) and  
37 models (Serreze et al., 2021). Several works have examined ROS frequency from the climatological point of  
38 view, by analyzing ROS spatial-temporal patterns for Alaska (Crawford et al., 2020), Japan (Ohba and Kawase,  
39 2020), Norway (Pall et al., 2019; Mooney and Li, 2021) or the Iberian Peninsula mountains (Morán-Tejeda et  
40 al., 2019). ROS events have also been linked with Northern-Hemisphere and Arctic low-frequency climate  
41 modes of variability (Rennert et al., 2009; Cohen et al., 2015) as well as synoptic weather types (Ohba and  
42 Kawase, 2020). Further, several works in mountain catchments of Switzerland (Würzer et al., 2016), Germany  
43 (Garvelmann et al., 2014a), United-States (Marks et al., 1992), Canadian Rockies (Pomeroy et al., 2016) or  
44 Spain (Corripio and López-Moreno, 2017), have portioned the contribution of Surface Energy Balance (SEB)  
45 components during ROS events. ROS alters snow and soil conditions, since the liquid water percolation creates  
46 ice layers and could alter the snowpack stability (Rennert et al., 2009). In severe ROS events, water percolation  
47 reaches the ground, and the subsequent water freezing causes latent heat releases, leading to soil and permafrost  
48 warming (Westermann et al., 2011). Positive heat fluxes during ROS events enhance snow runoff (Corripio  
49 and López-Moreno, 2017), especially in warm and wet snowpacks (Würzer et al., 2016). ROS can also trigger  
50 a snow avalanche in mountain zones (Conway and Raymond, 1993), flash flood events (Surfleet and Tullos,  
51 2013), impacts in tundra ecosystems (Hansen et al., 2013) and herbivore populations such as reindeers (Kohler  
52 and Aanes, 2004).

53

54 Different ROS frequency trends have been found since the last half of the 20<sup>st</sup> century. In the western United-  
55 States and from 1949 to 2003 (McCabe et al., 2007) found a general ROS frequency decrease in 1500 m but  
56 an increase in high elevations. Similarly, the analysis of six major German basins from 1990 to 2011, reveals  
57 an upward (downward) ROS frequency trend during winter (spring) at 1500 m and high elevations (Freudiger  
58 et al., 2014). On the contrary, from 1979 to 2014, no winter ROS frequency trends were found across the entire  
59 Northern-Hemisphere (Cohen et al., 2015). ROS projections for the end of the 21<sup>st</sup> century suggest a general  
60 ROS frequency increase in cold regions. This is projected for Alaska (Bieniek et al., 2018), Norway (Mooney  
61 and Li, 2021), western United-States (Musselman et al., 2018), Canada (il Jeong and Sushama, 2018) or Japan  
62 (Ohba and Kawase, 2020). In European mid-latitude mountain ranges, such as the Alps, ROS frequency is  
63 expected to increase (decrease) in high (low) elevation sectors (Beniston and Stoffel, 2016; Morán-Tejeda et

al., 2016). López-Moreno et al. (2021) compared the ROS sensitivity to climate warming across 40 global basins and detected the highest ROS frequency decreases in low-elevated and warm Mediterranean mountain sites. Despite the increasing understanding of ROS spatio-temporal past and future trends, little is known about the ROS sensitivity to climate warming across southern European mountain ranges, such as the Pyrenees. Here we examine the ROS sensitivity to temperature and precipitation change for low (1500 m), mid (1800 m) and high (2400 m) elevations of the Pyrenees. ROS responses to temperature and precipitation is analyzed using a physically based snow model, forced with reanalysis climate data perturbed according to 21<sup>st</sup> century climate projections spread for range (Amblar-Francés et al., 2020). Previous studies in alpine zones have shown different ROS response to warming depending on the area and month of the season (e.g., Morán-Tejeda et al. 2016). For this reason, results are focused on these two factors. First, we analyze height of snow (HS) and snowfall fraction (Sf) responses to temperature and precipitation since these are the main drivers of ROS (López-Moreno et al., 2021). Next, we examine ROS patterns and their response to warming by three key ROS indicators, namely:

77

- (a) Number of ROS days for a season (ROS frequency).
- (b) Average rainfall quantity during a ROS day (ROS rainfall amount).
- (c) Average daily snow ablation during a ROS day (ROS ablation).

81

The study area is presented in Section 2. Section 3 describes the data and methods. Section 4 presents the results. We finally discuss the anticipated ROS spatio-temporal changes, their socio-environmental impacts and hazards in Section 5.

85

## 86 **2 Regional setting**

87

The Pyrenees mountain range is located between the Atlantic Ocean (West) and the Mediterranean Sea (East), and is the largest (~ 450 km) mountain range of the Iberian Peninsula. Elevation increases towards the central massifs, where the highest peak is found (Aneto, 3,404 m asl). Glaciers expanded during the Little Ice Age and nowadays are located in the highest mountain summits (Vidaller et al., 2021). The regional annual 0 °C isotherm is at ca. 2700 m (Del Barrio et al., 1990), and at ca. 1600 m during the cold season (López-Moreno and Vicente-Serrano, 2011). The elevation lapse-rate is ca. 0.6°/100 m, being slightly lower during winter (Navarro-Serrano and López-Moreno, 2017). Annual precipitation is ca. 1000 mm/year (ca. 1500 m); maximum values are found in the northern-western massifs (around 2000 mm/year), decreasing towards the southern-eastern (SE) area (Lemus-Canovas et al., 2019). Precipitation is predominantly (> 90%) solid above 1600 m from November to May (López-Moreno, 2005). Due to the mountain alignment, relief configuration, and the distance to the Atlantic Ocean, seasonal snow accumulations in the northern slopes (ca. 500 cm/season), almost doubles the recorded in the SE area for the same elevation (ca. 2000 m) (Bonsoms et al., 2021b). In the western and central area of the southern slopes of the range (SW sector, Figure 1), snow accumulation is ruled by Atlantic wet and mild flows, which are linked with negative North Atlantic Oscillation (NAO) phases (SW

and W synoptic weather types) (López-Moreno, 2005; Alonso-González et al., 2020b; Bonsoms et al., 2021a). Positive Western Mediterranean Oscillation (WeMO) phases (NW and NE synoptic weather types) control the snow patterns in the northern-eastern (NE) slopes of the range (Bonsoms et al., 2021a). Generally, snow ablation starts in February in low elevations and in May at high elevation. The energy available for snow ablation is controlled by net radiation (55 %, over the total), latent (32 %) and sensible (13 %) heat fluxes (Bonsoms et al., 2022).

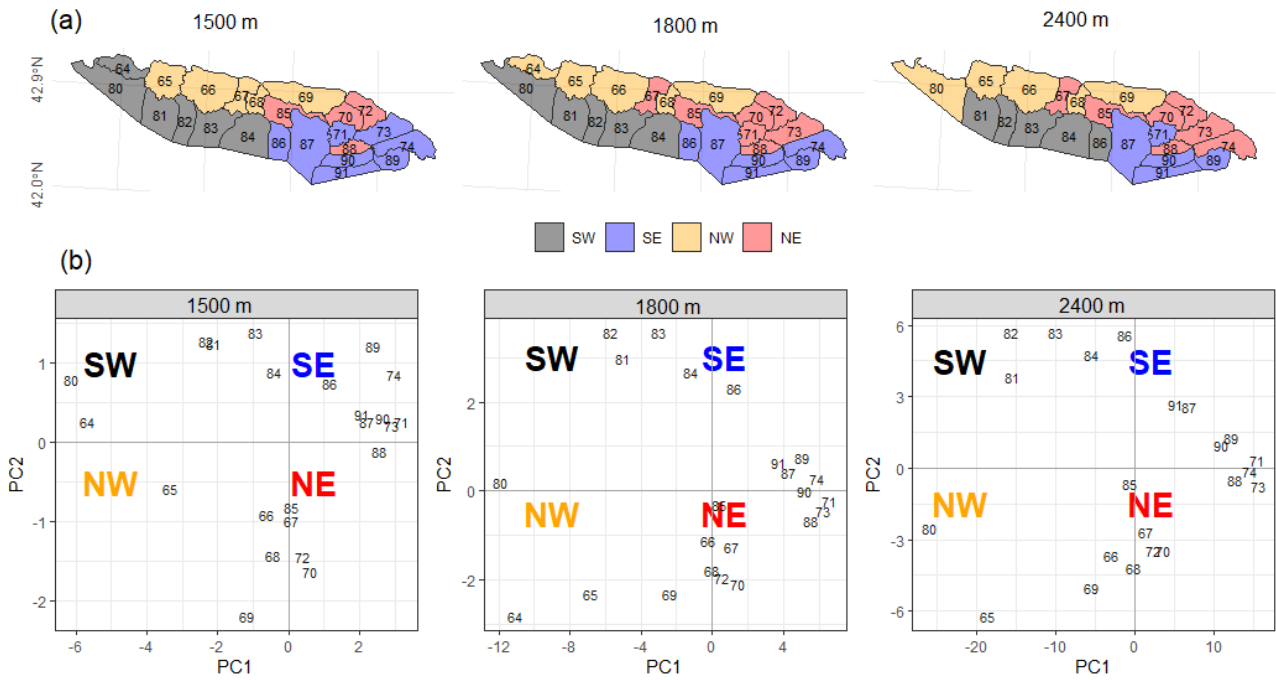


**Figure 1.** (a) Pyrenean massifs sectors (colors) for 1500 m, 1800 m and 2400 m elevation. (b) Principle Component Analysis (PCA) scores of each massif for 1500 m, 1800 m and 2400 m elevation. The black numbers are the SAFRAN massif's identity numbers defined by Vernay et al. (2022). Note that high elevation does not include massif number 64 since this massif does not reach 2400 m.

### 3 Data and methods

#### 3.1 Snow model description

Snowpack is modeled using the energy and mass balance snow model FSM2 (Essery, 2015). The FSM2 was forced at hourly resolution for each massif and elevation range (c.f. Sect. 3.3) for the baseline climate (1980 – 2019) according to climate projections (c.f. Sect. 3.4). Sf was quantified using a threshold-approach. Precipitation was snowfall when temperature was  $< 1$  °C according to previous ROS research in the study zone (Corripio and López-Moreno, 2017) and the average rain-snow temperature threshold for the Pyrenees (Jennings et al., 2018). Snow cover is calculated by a linear function of snow depth, snow albedo is estimated

127 based on a prognostic function with the new snowfall. Snow thermal conductivity is estimated based on snow  
128 density. Liquid water percolation is calculated based on a gravitational drainage. Compaction rate is simulated  
129 from overburden and thermal metamorphism. The atmospheric stability is estimated through the Richardson  
130 number stability functions to simulate latent and sensible heat fluxes. The selected FSM2 configuration  
131 includes three snow layers and four soil layers. The detailed FSM2 physical parameters and Fortran  
132 compilation numbers are shown in Table S1. The FSM2 model and configuration was previously validated in  
133 the Pyrenees at Bonsoms et al. (2023). FSM2 has been successfully used in snow model sensitivity studies in  
134 alpine zones (Günther et al., 2019). FSM2 has been implemented in a wide range of alpine conditions, such as  
135 for the Iberian Peninsula mountains (Alonso-González et al., 2019), Spanish Sierra Nevada (Collados-Lara et  
136 al., 2020) or swiss forest environments (Mazzotti et al., 2020) snowpack modeling. FMS2 has been integrated  
137 in snow data-assimilation schemes in combination with in-situ (Smyth et al., 2022) and remote-sensing data  
138 (Alonso-González et al., 2022).

139

### 140 **3.2 Atmospheric forcing data**

141

142 The FSM2 was forced with the SAFRAN meteorological system reanalysis dataset for flat terrain (Vernay et  
143 al., 2022). The SAFRAN meteorological system integrates meteorological simulations, remote-sensing cloud  
144 cover data, and instrumental records through data-assimilation. SAFRAN is forced with a combination of  
145 ERA-40 reanalysis (1958 to 2002) and the numerical weather prediction model ARPEGE (2002 to 2020).  
146 SAFRAN system was firstly designed for avalanche monitoring (Durand et al., 1999, 2009), but the accurate  
147 results obtained enhanced the diffusion of the meteorological system and its integration in the French  
148 hydrometeorological modelling system by the local weather service, Météo-France (Habets et al., 2008).  
149 SAFRAN has been extensively validated as meteorological forcing data for the snow modeling in complex  
150 alpine terrain (Revuelto et al., 2018; Deschamps-Berger et al., 2022), to study long-term snow evolution  
151 (Réveillet et al., 2022), avalanche hazard forecasting (Morin et al., 2020), snow climate projections (Verfaillie  
152 et al., 2018), snow depth (López-Moreno et al., 2020) and energy heat fluxes spatio-temporal trends (Bonsoms  
153 et al., 2022).

154

### 155 **3.3 Spatial areas**

156

157 SAFRAN system provides data at hourly resolution from 0 to 3600 m, by steps of 300 m, grouped by massifs.  
158 The SAFRAN massifs (polygons of Figure 1) were chosen for their relative topographical and climatological  
159 similarities (Durand et al., 1999). We selected the 1500 m (low), 1800 m (mid), and 2400 m (high) specific  
160 elevation bands of the Pyrenees. In order to retain the main spatial differences across the mountain range,  
161 reduce data dimensionality and include the maximum variance, massifs with similar interannual snow  
162 characteristics were grouped into sectors by performing a Principal Component Analysis (PCA). PCA is an  
163 extensively applied statistical method for climatological and snow spatial regionalization (i.e., López-Moreno  
164 and Vicente-Serrano, 2007; Schöner et al., 2019; Alonso-González et al., 2020a; Matiu et al., 2021; Bonsoms

et al., 2022). A PCA was applied over HS data for all months and years of the baseline climate. Massifs were grouped into four groups depending on the maximum correlation to the first (PC1) and second (PC2) scores. Pyrenean sectors were named South-West (SW), South-East (SE), North-West (NW) and North-East (NE) due to their geographical position. Figure 1 shows the resulting Pyrenean regionalization for 1500 m, 1800 m and high elevation as well as the SAFRAN massifs PC1 and PC2.

170

### 171 3.4 Sensitivity analysis

172

ROS season extension was defined according to ROS occurrence during the baseline climate period. For the purposes of this research, seasons are classified as follows: October and November (Autumn); December, January, and February (Winter); March, April, May, and June (Spring); and July (Summer). August and September are not included due to the absence of regular snow cover. ROS sensitivity to precipitation,  $T_a$ , increasing incoming longwave radiation ( $L_{win}$ ) accordingly. This method has been successfully applied and validated for analyzing the snow sensitivity to temperature and precipitation changes in many mountains, such as the Pyrenees (e.g., López-Moreno et al., 2013), the Iberian-Peninsula mountain areas outside the Pyrenees (Alonso-González et al., 2020a), Alps (Marty et al., 2017), Canadian basins (Pomeroy et al., 2015; Rasouli et al., 2019), or western United-States (Musselman et al., 2017b), among other works. This methodology has also been also performed in global ROS sensitivity to temperature change studies (López-Moreno et al., 2021). SAFRAN reanalysis climate data was perturbed according to Spanish Meteorological Agency climate change scenarios projected for the 21st Century in the Pyrenees (Amblar-Francés et al., 2020). Precipitation was increased (+10%), left unchanged (0 %) and decreased (- 10%).  $T_a$  (°C) was perturbed from +1°C to +4°C by +1°C.  $L_{win}$  was increased due to warming, by applying the Stefan-Boltzmann law, using the Stefan-Boltzmann constant ( $\sigma$ ;  $5.670373 \times 10^{-8} W m^{-2} K^{-4}$ ), and the hourly atmospheric emissivity ( $\epsilon_t$ ) derived from SAFRAN  $T_a$  and  $L_{win}$ :

189

$$\epsilon_t = \frac{LW_{in}}{\sigma(T_a + 273.15)^4}$$

191

A temperature increase of 1°C can be interpreted as an optimistic projection for the region, while 2°C and 4°C would represent projections for mid and high emission scenarios, respectively (Pons et al., 2015). The range of +/-10% for precipitation includes the expected changes in precipitation according to the vast majority of climate models, regardless of the emission scenario (López-Moreno et al., 2008; Pons et al., 2015; Amblar-Francés et al., 2020).

### 197 3.5 ROS definition and indicators

198

The average HS and Sf sensitivity to temperature and precipitation (expressed in % per °C) is the average seasonal HS and Sf anomalies under the baseline climate and divided by degree of warming. Days are classified as ROS days when daily rainfall amount was  $\geq 10$  mm and HS  $\geq 0.1$  m, according to previous works

(Musselman et al., 2018; López-Moreno et al., 2021). ROS frequency are the number of ROS days. ROS rainfall amount is the average daily rainfall (mm) during a ROS day. ROS ablation is the average daily snow ablation (cm) during a ROS day. The average daily snow ablation is the daily average HS difference between two consecutive days (Musselman et al., 2017a). Only the days when a negative HS difference occurred were selected. ROS exposure is the relation between ROS rainfall amount (y-axis) and ROS frequency (x-axis) differences from the baseline climate scenario for the massifs where ROS frequency is recorded for all increments of temperature.

209

## 210 **4 Results**

211

212 We provide an analysis of ROS drivers, near-present ROS patterns and their response to warming. ROS spatio-temporal dynamics are analyzed by frequency, rainfall quantity and snow ablation. Since we have detected a non-linear and counter-intuitive ROS sensitivity to temperature, ROS indicators values are shown for each increment of temperature, grouped by elevation and sectors, namely SW, SE, NW and NE.

216

### 217 **4.1 HS and Sf response to temperature and precipitation change**

218

219 HS and Sf response to temperature and precipitation is shown in Figure 2. Seasonal HS and Sf variability is mostly controlled by the increment of temperature, season, elevation, and spatial sector. The role of precipitation variability in the seasonal HS evolution is moderate to 1500 m (Figure S1 to S3). Only in 2400 m elevation an upward trend of precipitation (at least > 10%) can counterbalance small increments of temperature (< 1°C, over the baseline climate) from December to February (Figure S3). For this reason, precipitation was excluded to further analysis. Snow in 1500 m and 1800 m elevations during summer is rarely observed, however, marginal snow cover in 2400 m elevation can last until June and July, especially in the wettest sectors of the range (NW and SW). Seasonal HS and Sf response to temperature show large seasonality. The average HS decrease per °C ranges from 39 %, 37 % and 28 % per °C, for 1500 m, 1800 m and 2400 m elevations, respectively. However, relevant differences are found depending on the season and degree of warming (Figure 3). Maximum HS and Sf reductions are found in 1500 m and 1800 m elevations during the shoulders of the season (autumn and spring), coinciding with the time when ROS events are more frequent for the baseline climate (Figure 3). In these elevations, maximum HS decreases (52 % over the baseline climate) are modeled for spring when temperature is + 1°C. The greatest HS decreases in 2400 m elevation areas are modeled for summer (54 % HS decrease for 1°C). If temperature reaches maximum values (+ 4 °C), seasonal HS is reduced 92 %, 89 %, and 79 % for low, 1800 m, and 2400 m elevations, respectively (Figure S4).

235

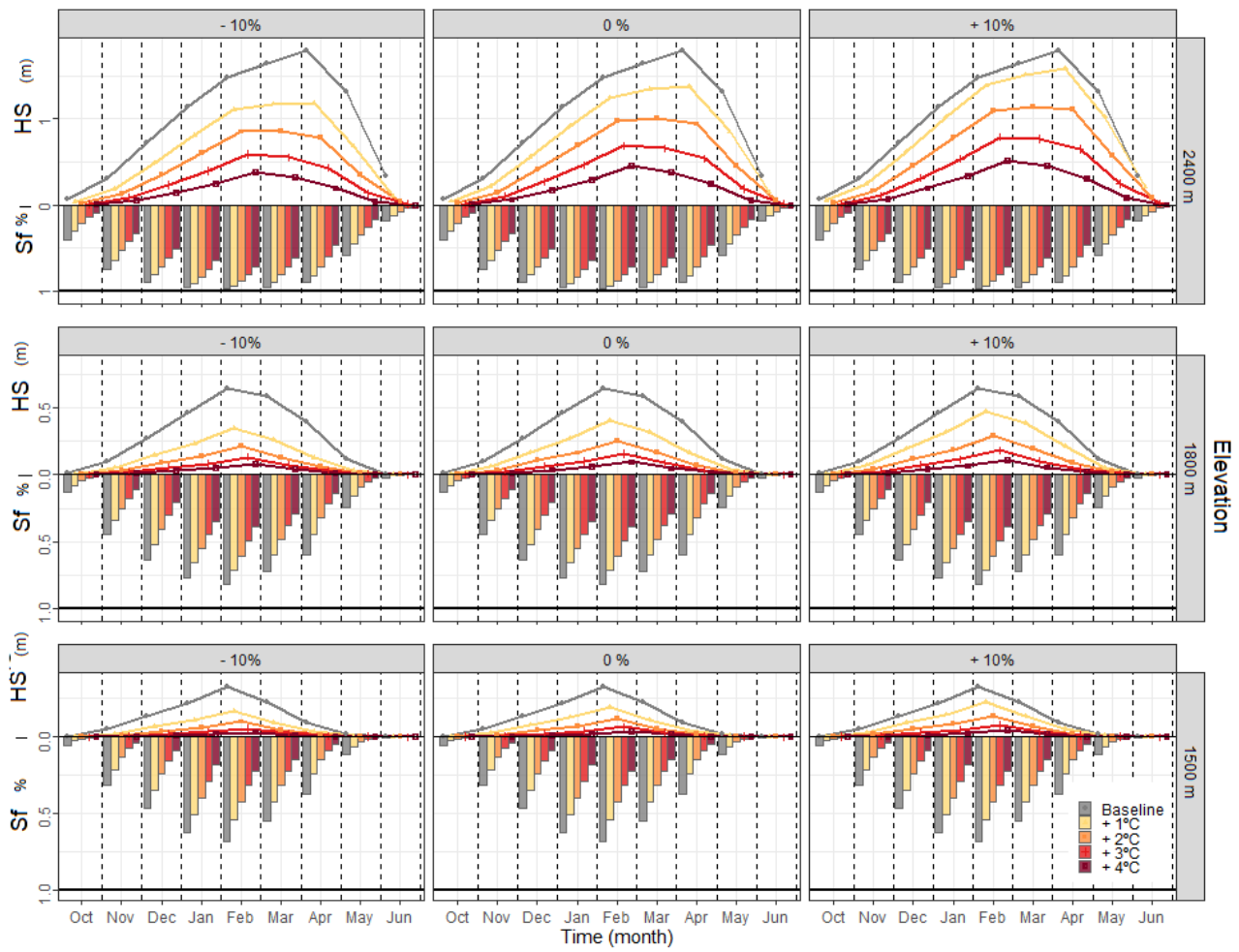


**Figure 2.** Height of snow (HS) (lines) and Snowfall fraction (Sf) (bars) monthly variation for baseline climate scenario and different increments of temperature (colors) grouped by elevation (rows) and sectors (columns).



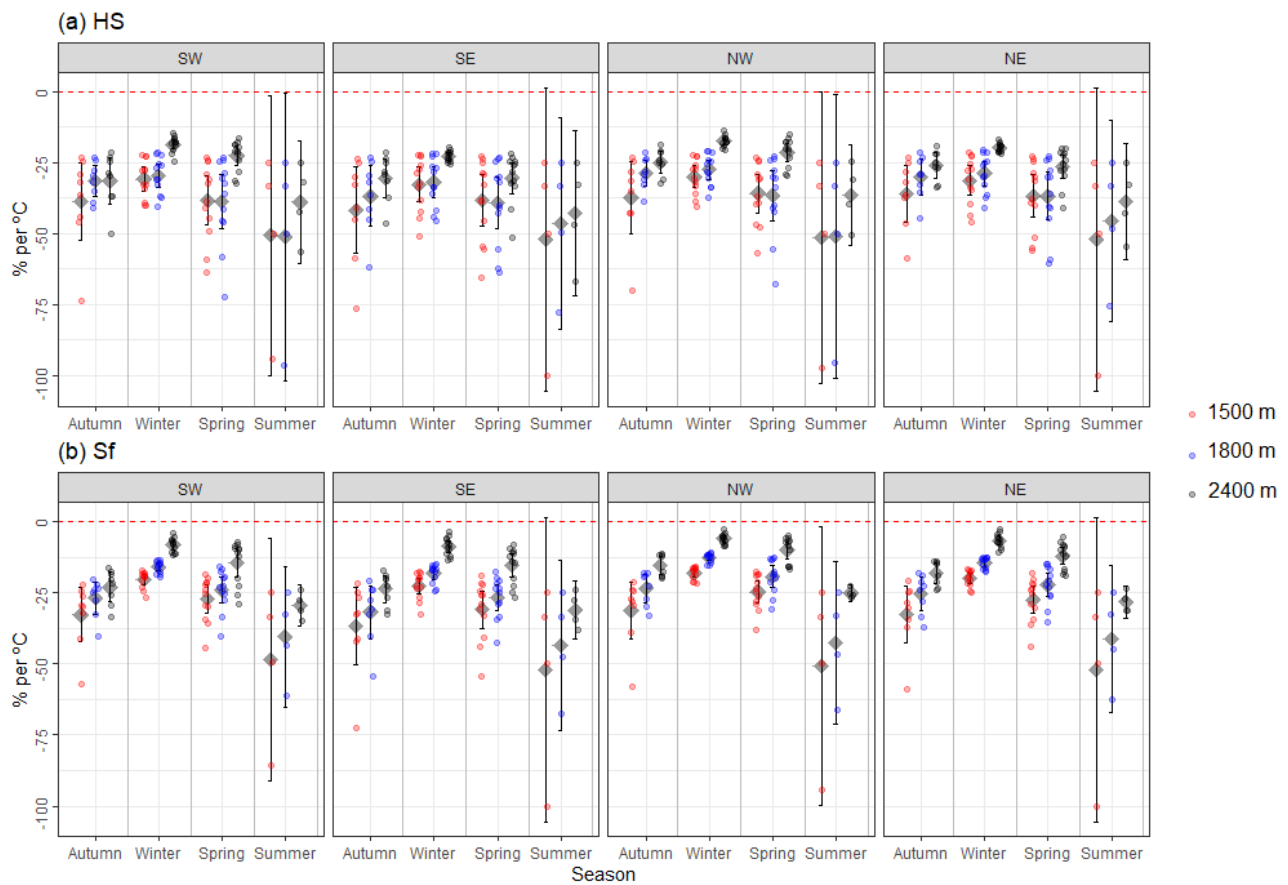


**Figure 3.** Seasonal (a) HS and (b) Sf anomalies over the baseline climate. Data are shown by elevation (colors), season (x-axis) and sectors (boxes). Points represent the average seasonal HS and Sf anomalies grouped by month of the season and increment of temperature (from 1°C to 4°C). The black diamond point indicates the mean, whereas the upper and lower error bars show the Gaussian confidence based on the normal distribution.

Sf shows lower sensitivity to warming than HS and maximum reductions in autumn. On average, Sf decreases by 29%, 22 %, and 12 % per °C for low, 1800 m, and 2400 m elevations, respectively. An increase of 4°C supposes Sf reductions of 80 %, 69 % and 49 % for low, 1800 m, and 2400 m elevations. Different HS and Sf sensitivity to temperature are found across the range. Independently of the elevation band and season, the SE exhibit the greatest HS and Sf decreases (41 % and 35 % per °C, respectively). On the contrary, minimum reductions are expected in the northern slopes (NW and NE).

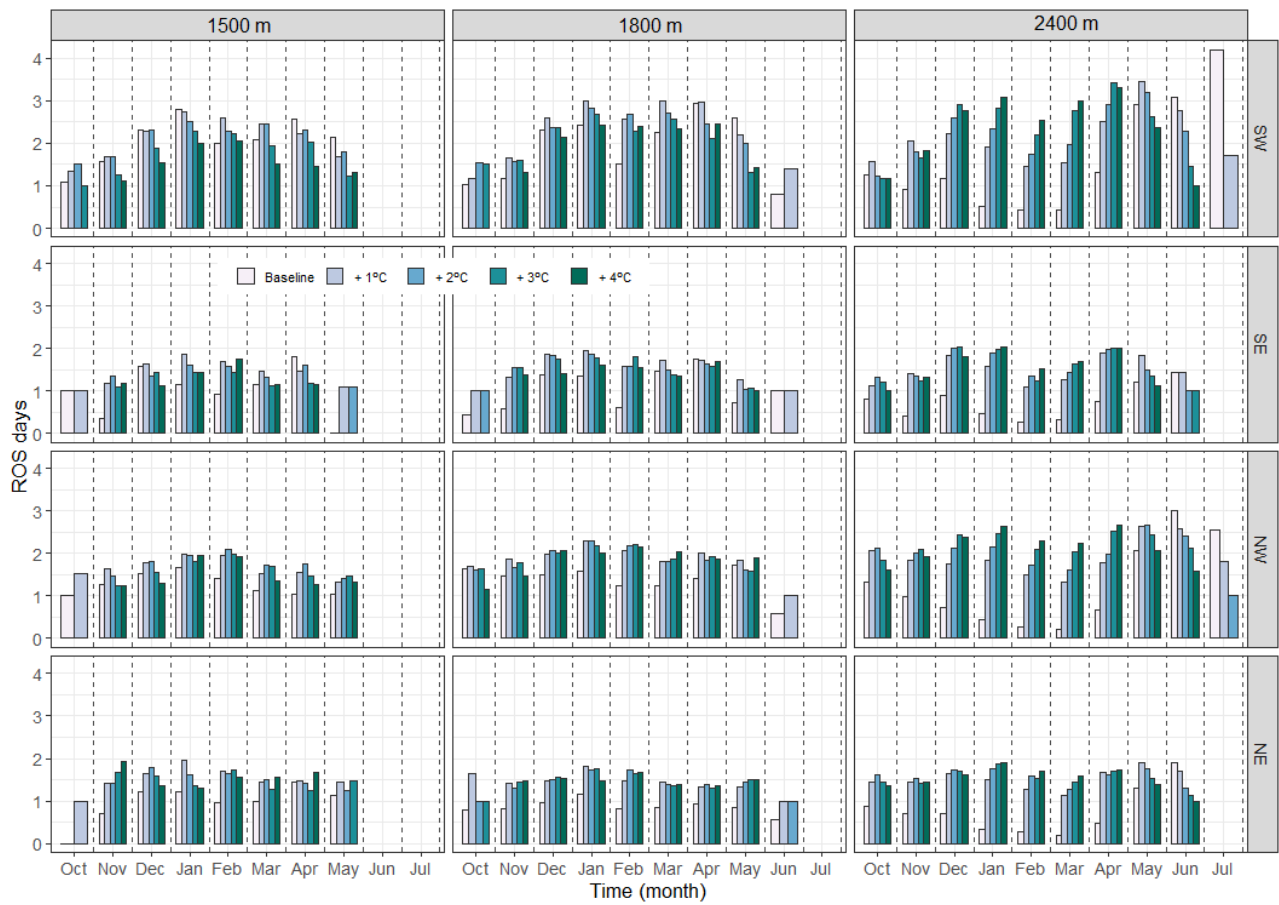
#### 4.2 ROS frequency

Low elevation annual ROS frequency for the baseline climate is 17, 8, 10 and 7 days/year for SW, SE, NW, NE sectors, respectively (Figure 4). The highest annual ROS frequency is however observed at 1800 m elevation. Here, annual ROS frequency is 17, 9, 12 and 9 for SW, SE, NW, NE sectors. Within these elevations, the maximum ROS frequency is detected in SW during winter and spring (7 days/season, for both elevations

263 and seasons). The eastern Pyrenees follow a similar seasonality. Maximum ROS frequency in 1500 m elevation  
 264 is found in winter (4 and 3 days/season, SE and NE, respectively), and during spring in 1800 m elevation (4  
 265 and 3 days, SE and NE, respectively). ROS is rarely observed in SE during the latest month of spring (May),  
 266 which contrast with the modeled values for SW (2 and 3 days/month, for 1500 m and 1800 m elevations,  
 267 respectively). 2400 m elevation shows the minimum ROS frequency. Here, comparisons between seasons  
 268 reveal maximum ROS frequency during summer, especially in SW (7 days/season), followed by NW (6  
 269 days/season), and NE (2 days/season).

270

271



272

273

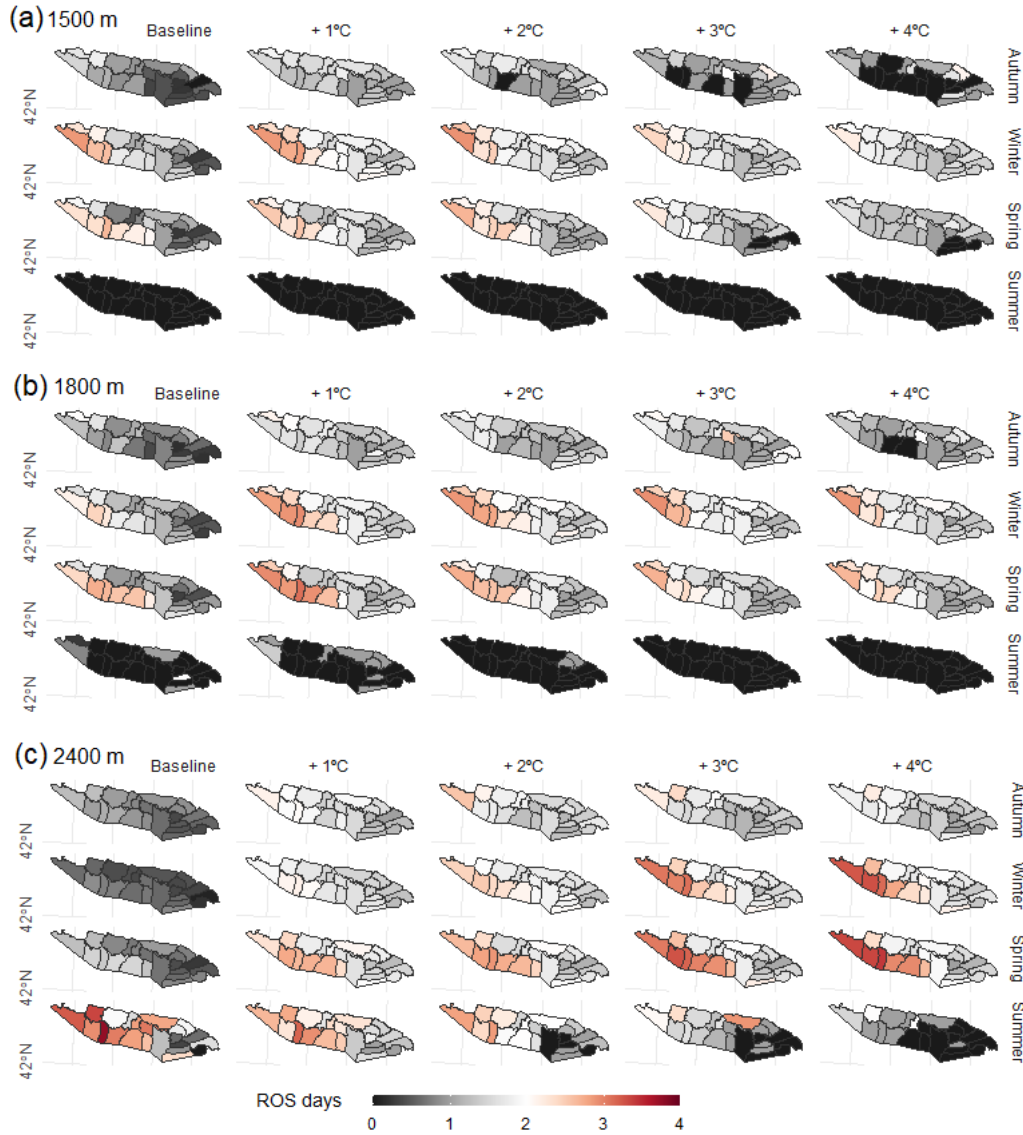
274 **Figure 4.** ROS frequency for baseline climate period (1980-2019) and increments of temperature, grouped  
 275 by months (x-axis), sector (rows) and elevation (columns).

276

277

278 ROS frequency response to warming vary depending on the month, increment of temperature, elevation, and  
 279 sector. ROS tends to disappear in October for 1500 m elevation except in SW (Figure 4 and 5). The highest  
 280 increases are seen during the winter for increments temperature lower than 3°C, particularly in NE, where ROS  
 281 frequency increases 1 day per month over the baseline scenario for + 1°C. In 1800 m elevation, ROS frequency  
 282 increases in all regions from November to February (around 1 day per month, for + 1°C up to + 3°C). Similar  
 283 increases are expected in NW and SW during the earliest months of spring and for 1500 m to moderate

284 increments of temperature. The contrary is observed during the latest months of spring in SW, where warming  
 285 reduces ROS events. A slight ROS frequency increase is found during spring for the rest of the sectors (Figure  
 286 4). ROS events in June are expected to disappear for temperature increases higher than 1°C. Finally, 2400 m  
 287 elevation shows the largest ROS frequency variations (around 1 day/month for + 1°C). Maximum ROS  
 288 frequency increases (3 days/month) are found in SW for more than + 3°C. ROS frequency progressively  
 289 increases in March and April for all sectors but tends to decrease in May (for + 3°C), June and July (for + 1°C).  
 290  
 291



292  
 293  
 294 **Figure 5.** Average ROS frequency (days) for a season for (a) 1500 m, (b) 1800 m and (c) 2400 m elevation.  
 295 Data are shown for the baseline climate period (1980-2019) and increment of temperature (left to right).  
 296

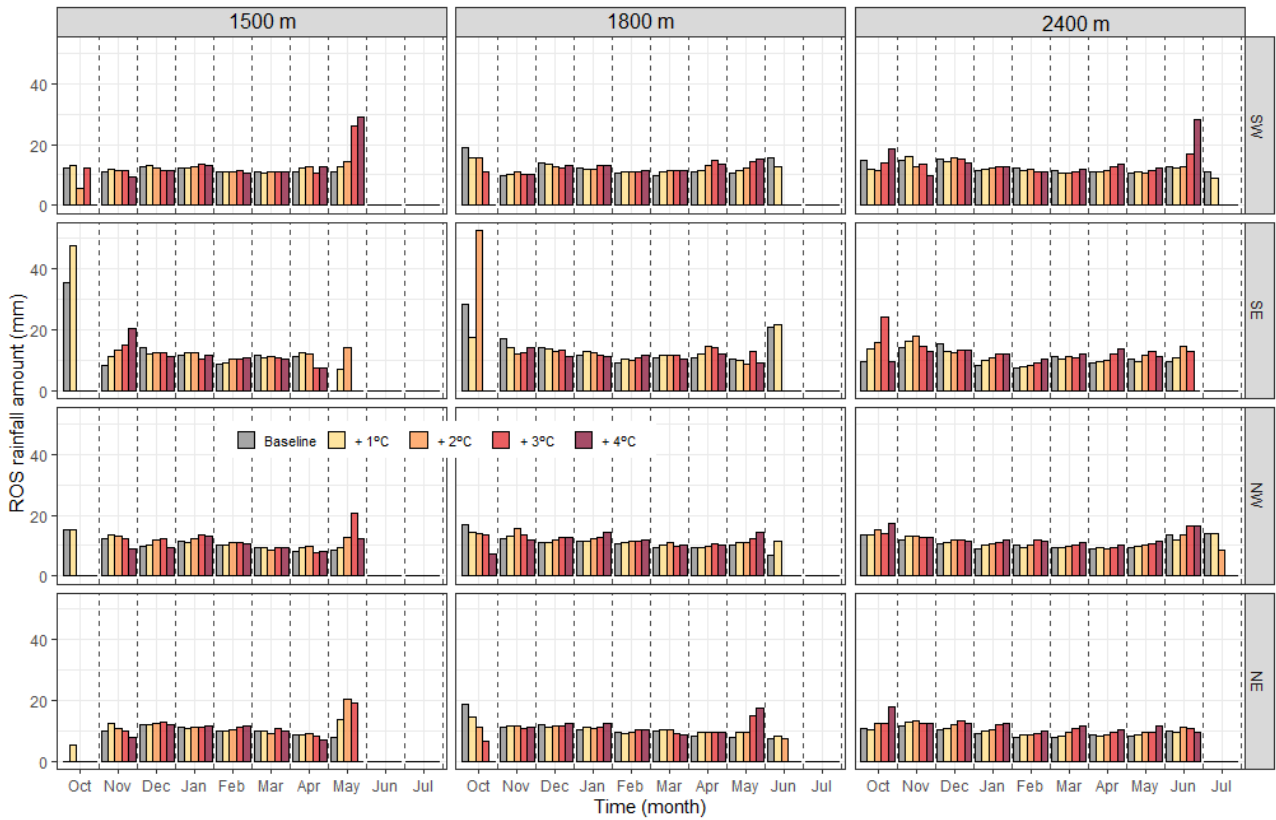
### 297 4.3 ROS rainfall amount

298  
 299 The spatial and temporal distribution of ROS rainfall amount is presented in Figure 6 and 7. The average 1500

300 m elevation ROS rainfall amount by year is 23, 28, 21, and 20 mm/day for SW, SE, NW, NE sectors,  
 301 respectively. Similarly, the highest values in 1800 m elevation are found in SE (29 mm/day, respectively). SE  
 302 sector experiences the highest ROS rainfall amount during autumn and summer (around 40 mm/day in 1500  
 303 m and 1800 m elevations. 2400 m elevation maximum ROS rainfall amount values are however found in the  
 304 western Pyrenees during the onset and offset snow season. Here, the largest ROS rainfall amount spatial and  
 305 seasonal distribution ranges from SW (29 mm/day, autumn), NW (28 mm/day, summer), SE (24 mm/day,  
 306 autumn) to NE (23 mm/day, autumn).

307

308



309

310

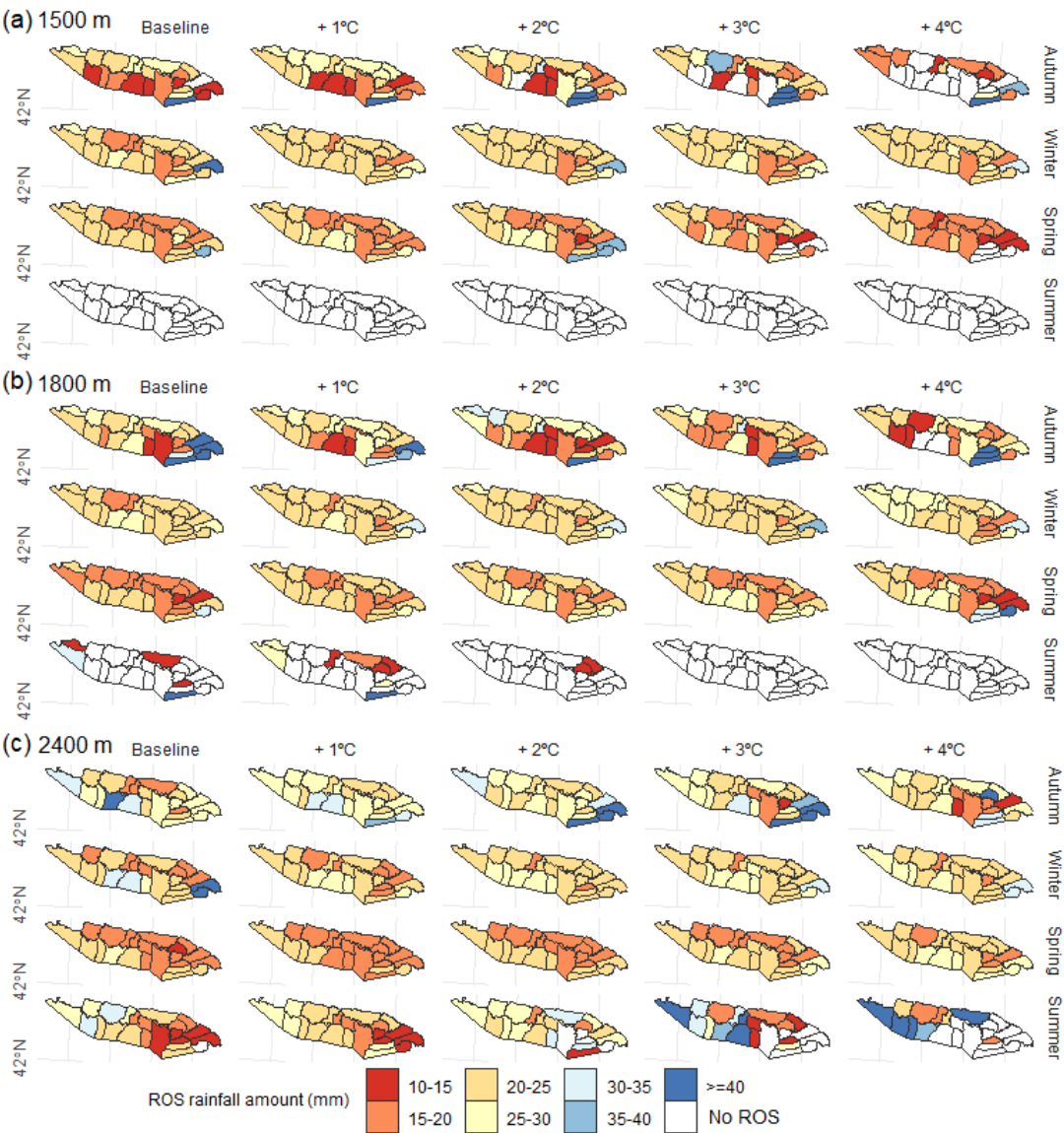
311

312 **Figure 6.** ROS rainfall amount (mm) temporal evolution for baseline climate (1980-2019) and increment of  
 313 warming (colors), grouped by elevation (columns) and sector (rows).

314

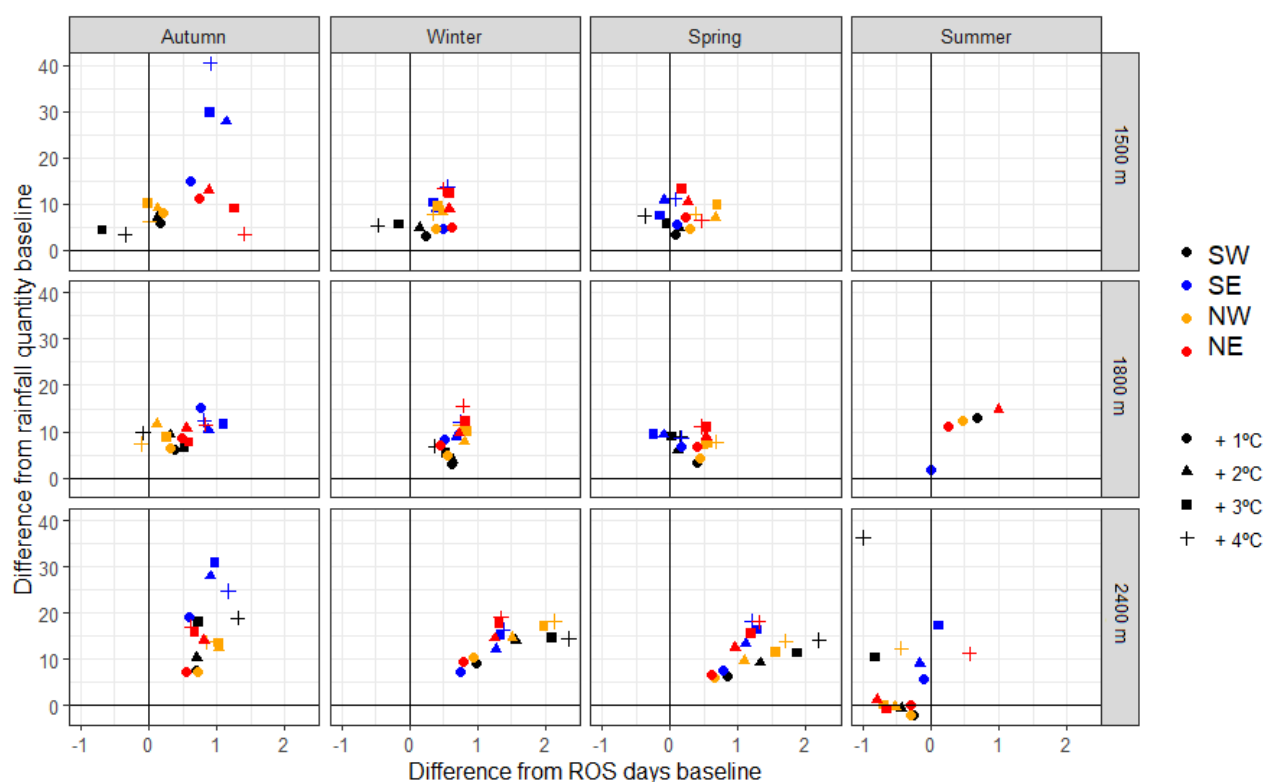
315 ROS rainfall amount progressively increases due to warming (4%, 4%, and 5% per °C for low, 1800 m, and  
 316 2400 m elevations, respectively; Table S2). Small differences are found by elevation and sector. 1500 m  
 317 elevation ROS rainfall amount increases until + 3°C, and generally decreases for + 4°C during the earliest  
 318 (October to December) and latest (April and May) months of the snow season. Similar patterns are found in  
 319 1800 m elevation. ROS rainfall amount increases up to + 4°C, except in the SE sector for specific months  
 320 (Figure 6). The latter sector shows also maximum ROS rainfall amount values in autumn due to torrential  
 321 rainfall. 2400 m elevation ROS rainfall amount increase at a constant rate of around 5 % per °C. Yet, maximum

322 increases are modeled in SW during summer, when ROS rainfall amount almost doubles the baseline climate  
 323 (+ 40% for + 4°C).  
 324  
 325



326  
 327 **Figure 7.** Average ROS rainfall amount (mm) for a season for (a) 1500 m, (b) 1800 m and (c) 2400 m  
 328 elevation. Data are shown for the baseline climate period (1980-2019) and increment of temperature (left to  
 329 right).  
 330  
 331 Data suggest that ROS exposure generally increases for all elevations and sectors during winter (except in SW  
 332 for temperatures greater than 3°C). Nonetheless, remarkable spatial and seasonal differences are found. SE  
 333 show the maximum values in autumn. On the contrary, small changes in frequency are detected in SW and  
 334 NW, despite ROS rainfall amount is expected to increase ( $< 10\text{mm/day}$ ). For the majority of sectors and  
 335 elevations, ROS exposure generally increases in winter and spring. The minimum differences between sectors  
 336 are detected in these seasons. In summer, ROS exposure tends to generally decrease for all elevations under  
 337 severe warming due to snow cover depletion.

338  
339



340  
341  
342  
343  
344  
345  
346  
347

**Figure 8.** Average ROS exposure. Points are obtained by a scatterplot between ROS rainfall amount difference from baseline climate period (1980-2019) (y-axis) and ROS days difference from baseline climate (x-axis). Data is calculated by the average difference between (a) the baseline scenario (1980-2019) and (b) the different perturbed scenarios, only for the massifs where ROS frequency exists on (a) and (b). Data are shown for each season (columns), elevation (rows), sector (color) and increment of temperature (point shape).

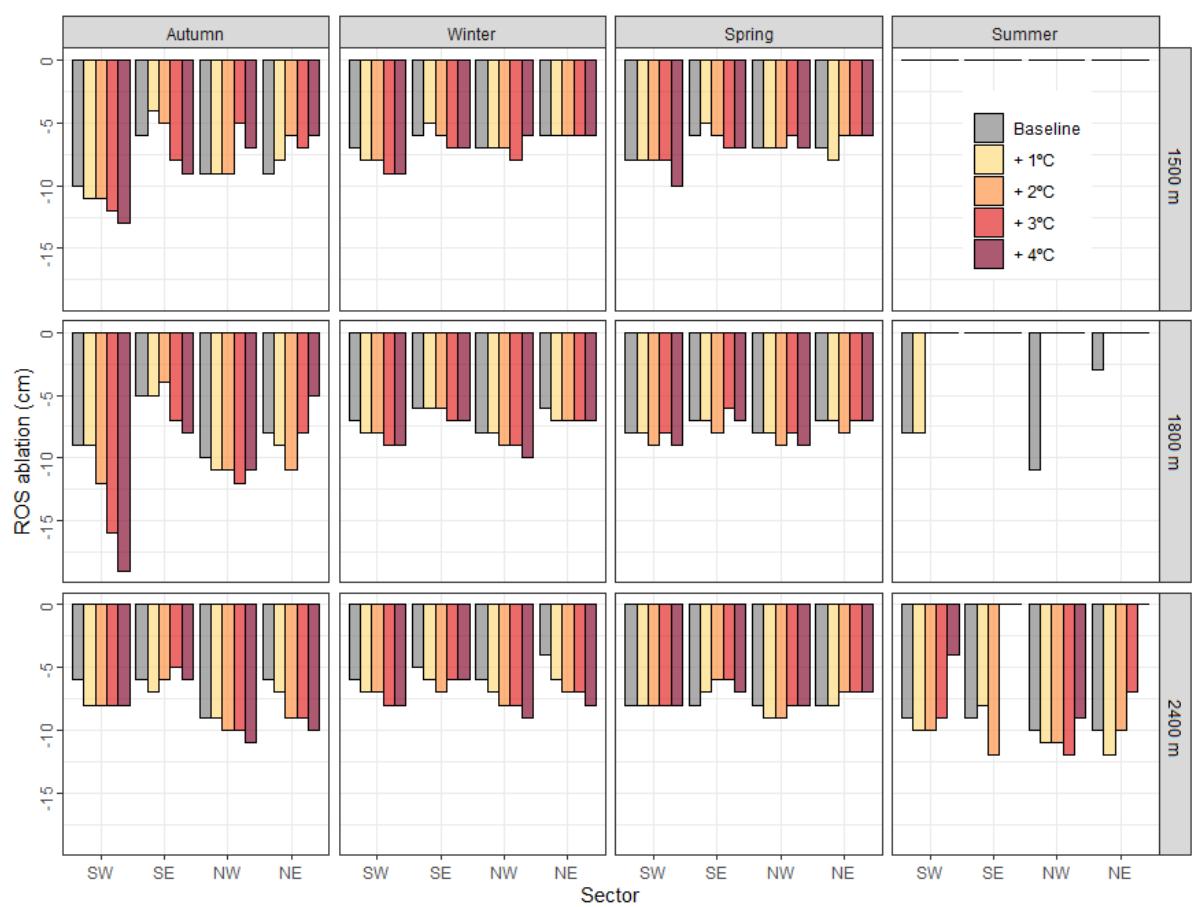
**4.4. ROS ablation**

349

ROS ablation is presented at Figure 9 and 10. ROS ablation ranges from -10 cm/day in NW 2400 m elevation (summer) to - 5 cm/day in NE 2400 m elevation (winter). ROS ablation nearly doubles the average daily snow ablation for all days on a season (Figure S5). Comparison with the reference baseline period reveals contrasting ROS ablation changes depending on the season, elevation and sector. Overall ROS ablation progressively increases due to warming in coldest zones and months of the season. The largest ROS ablation increments are detected in autumn and winter. For the former, ROS ablation increases at a generally constant rate in SW (11 %) NE (19 %) and NW (4 % per °C). For the latter, ROS ablation increases also in SW (11 %), NW (14 %) and NE (34 % per °C). In detail, maximum ROS ablation due to warming is found for 1800 m elevation during autumn (Figure 9). ROS ablation exhibit slow and no-changes in the warmest zone (SE), as well in the warmest months of the season, regardless the elevation band.

360

361  
362

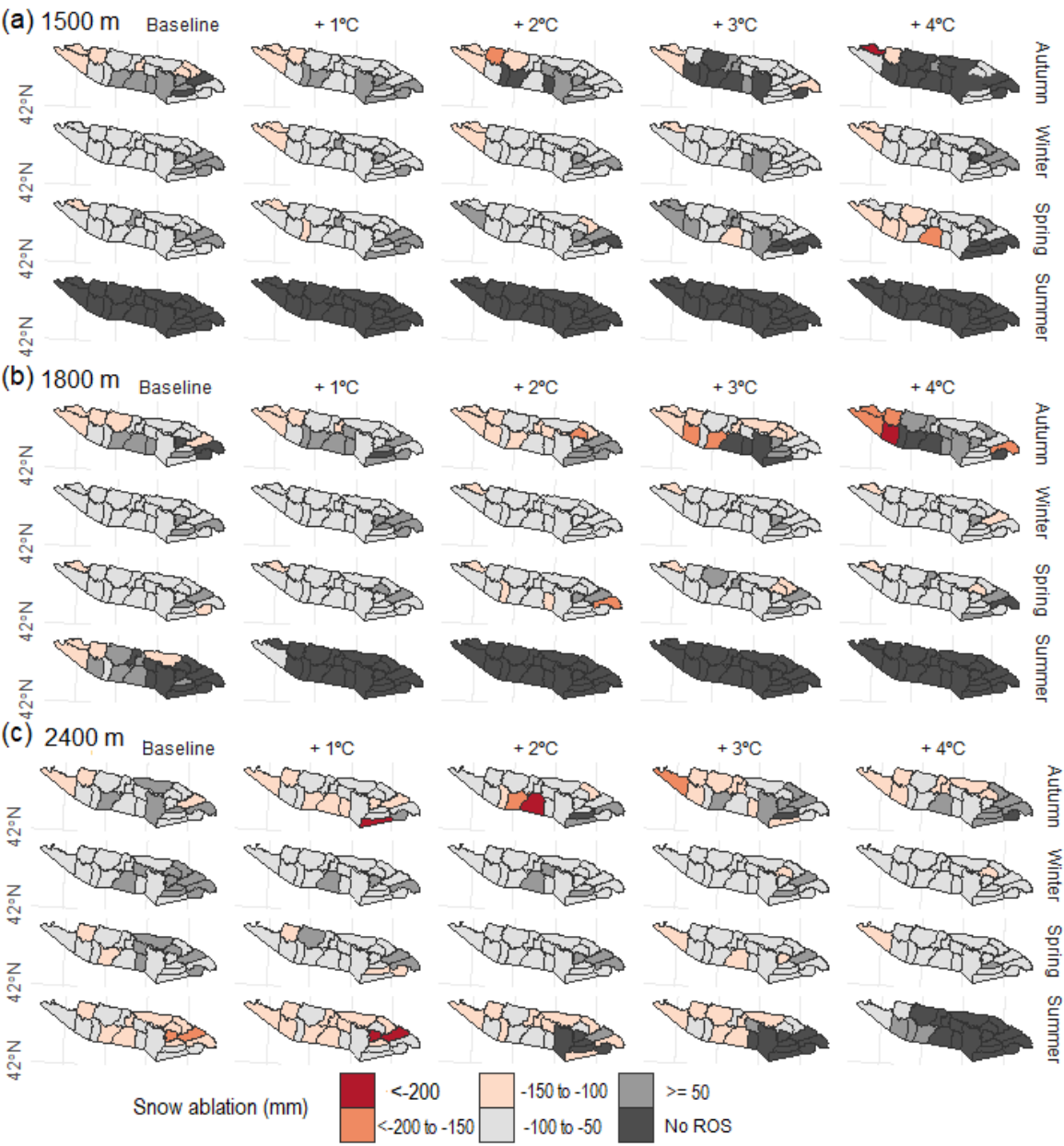


363  
364  
365

**Figure 9.** ROS ablation (y-axis) for baseline climate period (1980-2019) and increment of temperature (colors), sector (x-axis), season (columns) and elevation (rows).



366  
367



368  
369

370 **Figure 10.** Average ROS ablation for a season for (a) 1500 m, (b) 1800 m and (c) 2400 m elevation. Data are  
371 shown for the baseline climate period (1980-2019) and increment of temperature (left to right).

372

373 **5 Discussion**

374

375 The Pyrenees experienced a statistically significant positive temperature trend since the 1980s (ca. + 0.2  
376 °C/decade) but no statistically significant precipitation trends are detected (OPCC, 2018) due to strong spatial  
377 (Vicente-Serrano et al., 2017), inter-annual and long-term variability of the latter (Peña-Angulo et al., 2021).  
378 Depending on the study period different snow trends were found. From ca. 1980 to 2010, non-statistically



379 significant snow days and snow accumulation positive trends were generally detected at > 1000 m (Buisan et  
380 al., 2016), 1800 m (Serrano-Notivol et al., 2018), and > 2000 m (Bonsoms et al., 2021a). Long-term trends  
381 (1957 to 2017), however, reveal statistically-significant snow depth decreases at 2100 m, but large variability  
382 depending on the sector and the snow indicator (López-Moreno et al., 2020). Climate projections for the end  
383 of the 21<sup>st</sup> century suggest an increase of temperature (> 3°C), together with 1500 m precipitation shifts (<  
384 10%) from autumn to spring (Amblar-Francés et al., 2020). Within this climate context, ROS spatio-temporal  
385 patterns will likely change. In order to anticipate future scenarios, ROS sensitivity to warming was analyzed  
386 through three key indicators of frequency, rainfall intensity and snow ablation.

387

## 388 5.1 ROS spatial variability

389

390 The climatic setting of the Pyrenees as well as its relief configuration determines a remarkable spatial and  
391 temporal variability of ROS events. The contradiction between rainfall ratio increases and snowpack  
392 reductions, as well as the 2400 m spatial and monthly differences found, explain the complex ROS response  
393 to warming. HS decrease by 39 %, 37 % and 28 % per °C, for 1500 m, 1800 m and 2400 m elevations,  
394 respectively. Similarly, Sf decreases by 29 %, 22 %, and 12 % per °C for 1500 m, 1800 m, and 2400 m  
395 elevations, respectively, providing evidence of an elevation-dependent snow sensitivity to temperature change.  
396 HS and Sf maximum reductions are reached for 1°C of warming, suggesting non-linear HS decreases, in  
397 accordance with previous snow sensitivity to climate change reported in central Pyrenees (López-Moreno et  
398 al., 2013). In detail, SW and NW annual ROS frequency almost doubles (17 and 12 days/year, respectively)  
399 the one recorded in SE and NE (9 days/year, for both sectors). Maximum ROS frequency for a season are  
400 found in SW and NW because of larger snow magnitudes in this sector (i.e., López-Moreno, 2005; López-  
401 Moreno et al, 2007; Navarro-Serrano et al., 2017; Bonsoms et al., 2021a). Thus, snow cover last longer until  
402 spring when minimum Sf values are found (Figure S1). This sector is the most exposed to SW and W air flows  
403 (negative NAO phases) (López-Moreno, 2005), which bring wet and mild conditions over the mountain range,  
404 leading to most ROS-related floods in the range (Morán-Tejeda et al., 2019). The generally ROS rainfall  
405 amount increase reported in this work (independently of the increment of temperature and elevation) is  
406 explained by the Sf reduction expected for all sectors (Figure 3). Maximum ROS rainfall amount is generally  
407 detected in spring (May), except in NE 2400 m elevation zones and SE (all elevations). In the latter sectors,  
408 ROS rainfall amount tends to disappear in October under large (> 2°C) increments of temperature. The seasonal  
409 snow accumulation in NE and SE is lower-than-average due to the lower influence of Atlantic climate in these  
410 sectors of the range. Hence, large increments of warming decreases ROS frequency due to snow cover  
411 depletion in early autumn and late spring (Figure S1). In addition, SE is closer to the 0°C due to higher-than-  
412 average sublimation, latent and radiative heat fluxes (Bonsoms et al., 2022) and for this reason in this sector  
413 each increment of temperature has larger effects on the Sf, HS and ROS frequency reduction (Figure 3). 2400  
414 m elevation show the largest variation over the baseline climate as well as ROS exposure because of the larger  
415 snowpack magnitude and duration compared to 1500 m and 1800 m areas. Thus, 2400 m elevation snow  
416 duration last until spring and summer, when the largest shift from snowfall to rainfall is found. On the other

hand, 1800 m elevation shows the maximum ROS rainfall amount since the amount of moisture for condensation decreases while air masses increase height (Roe and Baker, 2006). Furthermore, the largest ROS rainfall amount is detected in SE during autumn (Figure 7), because of the exposure of this region to Mediterranean low-pressure systems (negative WeMO phases), that usually trigger heavy rainfall events during this season (Lemus-Canovas et al., 2021).

## 5.2 ROS temporal evolution

Recent ROS trends in other mid-latitude areas are in accordance with ROS analysis presented here. Freudiger et al. (2013) analyzed the ROS trends (1950–2011 period) of the Rhine, Danube, Elbe, Weser, Oder, and Ems (Central Europe) basins. They found an overall ROS frequency increase during January and February (1990 to 2011 period), which is consistent with the ROS rainfall amount and frequency increase detected in winter for the Pyrenees for all elevations and increment of temperature. Similarly, in Sitter River (NE Switzerland), a ROS frequency increase of around 40% (200%) at <1500 m (>2500 m) was detected between 1960 and 2015 (Beniston and Stoffel, 2016). During the last half of the 20<sup>th</sup> century, ROS frequency trends show an upward (downward) trend in high (low) elevation in western United-States (McCabe et al., 2007), as well as in southern British Columbia (Loukas et al., 2002) and at catchment scale in Oregon (United-States) (Surfleet and Tullos, 2013). Same ROS frequency increases (decreases) has been detected from 1980 to 2010 in Norwegian high (low) elevated mountain zones (Pall et al., 2019). However, in contradiction with our results and previous studies, winter Northern-Hemisphere ROS frequency trends (1979-2014 period) show no-clear trends (Cohen et al., 2015).

Results exposed in this work provide more evidence of ROS frequency increases in high-elevation zones, as it has been suggested by climate projections and ROS sensitivity to temperature studies. ROS show an elevation-dependent pattern that was previously reported in the Swiss Alps (Morán-Tejeda et al., 2016). In Sitter River (NE Switzerland), an increase of 2 to 4 °C over the 1960 to 2015 period results in an increase of the ROS frequency by around 50% at > 2500 m (Beniston and Stoffel, 2016). Likewise, 21st century high-emission scenarios (RCP8.5), suggest increases in ROS frequency and intensity in Gletsch (Switzerland) high-elevation area; however, on climate projections for ROS definitions that include snow melting (Musselman et al., 2018), natural climate variability contributes to a large extend (70 %) of ROS variability (Schirmer et al., 2022). Li et al. (2019) analyzed the future ROS frequency in the conterminous United-States and detected a nonlinear trend ROS due to warming, which is consistent with the different ROS rainfall amount and frequency responses depending on the increment of temperature detected in our work. Climate projections for the mid-end of the 21<sup>th</sup> century projected positive ROS frequency and rainfall trends in Western United-States and Canada (Jeong and Sushama, 2018). Similarly, ROS frequency will likely decrease (increase) in the warmest months of the season in low (high) elevation areas of western United-States (Musselman et al., 2018). The same is projected Norwegian mountains (Mooney and Li, 2021). López-Moreno et al. (2021) analyzed 40 worldwide basins ROS sensitivity to warming. In their study they found a decrease of ROS events in warm mountain

455 areas. However, they detected ROS frequency increases in cold-climate mountains where large snow  
456 accumulation is found despite warming. In accordance with our results, they identified large seasonal  
457 differences and ROS frequency decreases in Mediterranean mountains due to snow cover depletion in the last  
458 months of the snow season.

459

### 460 **5.3 ROS ablation**

461

462 Warming increases ROS ablation from autumn to winter on deep snowpacks and in the coldest sectors of the  
463 range, due to higher energy for snow ablation and closer 0°C isotherm conditions in a warmer than baseline  
464 climate. Nevertheless, data show 1500 m or decreases in ROS ablation in SE and spring, since the snowpack  
465 is already near to the isothermal conditions. These results go in line with results modelled for cold and warm  
466 Pyrenean sites (López-Moreno et al., 2013) as well as for different Northern-Hemisphere sites (Essery et al.,  
467 2020). ROS ablation indicator is also indirectly affected by the HS magnitude decreases (30 % per °C; Figure  
468 3), and therefore lower ROS ablation is directly affected by lower HS magnitudes. Previous literature pointed  
469 out that warming have counter-intuitive effects on snow ablation patterns. Higher than average temperatures  
470 advance the peak HS date on average 5 days per °C in 1800 m and 2400 m elevations (Bonsoms et al., 2022b),  
471 triggering earlier snow ablation onsets, and therefore lower solar radiation fluxes (López-Moreno et al., 2013;  
472 Lundquist et al., 2013; Pomeroy et al., 2015; Musselman et al., 2017a; Sanmiguel-Valladolid et al., 2022), as  
473 well as earlier snow depletion before the maximum advection of heat fluxes into the snowpack (spring)  
474 (Bonsoms et al., 2022). Slower snow melt rates in a warmer climate have been detected in Western United-  
475 States (Musselman et al., 2017), as well as the entire Northern-Hemisphere (Wu et al., 2018). 1500 m or  
476 inexistent changes in snow ablation on warm and marginal snowpacks has been previously detected in the  
477 central Pyrenees (López-Moreno et al., 2013), in forest and open areas (Sanmiguel-Valladolid et al., 2022), in  
478 the entire range (Bonsoms et al., 2022), and other Iberian Peninsula Mountain ranges outside the Pyrenees  
479 (Alonso-González et al., 2020a).

480 ROS ablation is larger than the average snow ablation during a snow ablation day (Figure S6) due to higher  
481 SEB positive fluxes. Several works analyzed SEB changes on ROS events, and different SEB contributions  
482 has been found depending on the geographical area (Mazurkiewicz et al., 2008; Garvelmann et al., 2014b;  
483 Würzer et al., 2016; Corripio and López-Moreno, 2017; Li et al., 2019), ranging from net radiation in Pacific  
484 North West (Mazurkiewicz et al., 2008) to Lwin and turbulent heat fluxes in conterminous United-States  
485 mountain areas (Li et al., 2019) or the Swiss Alps (e.g., Würzer et al., 2016). In general, studies in mid-latitude  
486 mountain ranges have shown that turbulent heat fluxes contribute between 60 and 90 % of the energy available  
487 for snow ablation during ROS days (e.g., Marks et al., 1998; Garvelmann et al. 2014; Corripio and López-  
488 Moreno, 2017). In the central Pyrenees (> 2000 m) the meteorological analysis of a ROS event reveals that  
489 ROS ablation is larger than a normal ablation day because of the large advection of Lwin and especially  
490 sensible heat fluxes (Corripio and López-Moreno, 2017). Lwin increases due to the high cloud cover and warm

air, as it is frequently observed during ROS episodes (Moore and Owens, 1984). Further works should analyze the SEB controls during ROS events within the entire mountain range, as well as the ROS hydrological responses to climate warming.

#### **5.4 ROS socio-environmental impacts and hazards**

Temperature-induced changes in the seasonal snowpack and during ROS days suggest several hydrological shifts including, but not limited to, earlier peak flows on the season (Surfleet and Tullos, 2013), rapid streamflow peaks during high precipitation events in frozen soils (Shanley and Chalmers, 1999), faster soil moisture depletion and lower river discharges in spring due to earlier snow melt in the season (Stewart, 2009). The shortening of the snow season due to warming reported in this work will potentially alter alpine phenological patterns (i.e., Wipf and Rixen, 2010) and expand forest cover (Szczypka et al., 2015). Although vegetation branches intercept a large amount of snowfall, intermediate and high vegetation shields short-wave radiation, reduces snow wind-transport and turbulent heat fluxes (López-Moreno and Latron, 2008; Sanmiguel-Valellado et al., 2022). Snow-forest interactions, their sensitivity to climate change as well as the ROS hydrological response within a changing landscape is far from understood across the range and should be the base of forthcoming works.

The higher ROS exposure (Figure 8) will likely imply an increase of ROS-related hazards and impacts in the mountain ecosystem. Heavy ROS rainfall amount changes snow metamorphism on saturated snowpacks and leads to high-speed water percolation (Singh et al., 1997). The subsequent water refreezing changes the snowpack conditions and creates an ice-layer in the snowpack that can reach the surface (Rennert et al., 2009). ROS can cause plant damage (Bjerke et al., 2017) and the ice encapsulation of vegetation in tundra ecosystems can trigger severe wildlife impacts, such as vertebrate herbivores starvation (Hansen et al 2013), reindeer population mortality (Kohler and Aanes, 2004) and higher competition between species (Hansen et al 2014). Nevertheless, any study to the date analyzed ROS-related impacts in flora and fauna across Southern-European mountains. Snow albedo decay due positive heat fluxes and rainfall in ROS events (Corripio and López-Moreno, 2017), lead to faster snow ablation even on the next days (e.g., Singh et al. 1997). The combination of changes in internal snowpack processes, larger ROS rainfall amount, and more energy to ablate snow during spring could enhance snow runoff, especially during warm and wet snowpack conditions (Würzer et al., 2016). In snow-dominated regions ROS can lead to a specific type of avalanching (Conway and Raymond, 1993) and floods (Surfleet and Tullos, 2013). The latter are the most environmental damaging risk in Spain (Llasat et al., 2014) and around 50% of the flood in the Iberian Peninsula are due to ROS events (Morán-Tejeda et al., 2019). More than half of the historical (1940 to 2012) flood events in the Ésera river catchment (central Pyrenees) occurred during spring (Serrano-Notivol et al., 2017), which coincides with the snow ablation season. ROS floods have also economic impacts. For instance, a ROS flood event that occurred on 13<sup>th</sup> June of 2013 in the Garonne River (Val d'Aran, central Pyrenees) cost approximately 20 million of euros to the public insurance (Llasat et al., 2014).

527

## 528 **5.5 Limitations**

529

530 This study evaluates the sensitivity of ROS responses to climate change, enabling a better understanding of  
531 the non-linear ROS spatiotemporal variations in different sectors and elevations of the Pyrenees. Instead of  
532 presenting diverse outputs from climate model ensembles (López-Moreno et al., 2010), we provide ROS  
533 sensitivity values per 1°C, making them comparable to other regions and seasons. The temperature and  
534 precipitation change values used in this sensitivity analysis are based on established climate projections for the  
535 region (Amblar-Francés et al., 2020). However, precipitation projections in the Pyrenees exhibit high  
536 uncertainties among different models, GHGs emission scenarios, and temporal periods (López-Moreno et al.,  
537 2008).

538

539 The SAFRAN meteorological system used in this work relies on a topographical spatial division and exhibit  
540 and accuracy of around 1 °C in Ta and around 20 mm in the monthly cumulative precipitation (Vernay et al.,  
541 2022). Precipitation phase partitioning methods are subject to uncertainties under close-to-isothermal  
542 conditions (Harder et al., 2010). Hydrological models are also subject to errors in the snowpack prediction  
543 (Essery, 2015). However, the FSM2 is a multiphysics snowpack model that has been validated previously in  
544 the Pyrenees (Bonsoms et al., 2023) and compared against different snowpack models (Krinner et al., 2018),  
545 providing evidence of its robustness.

546

## 547 **6 Conclusions**

548 The expected decreases in Sf and HS due to climate warming will likely change ROS spatio-temporal patterns  
549 across the Pyrenees. Therefore, a better understanding of ROS is required. This work analyzed the ROS  
550 sensitivity to warming by forcing a physically based snow model with perturbed reanalysis climate data (1980-  
551 2019 period) for 1500 m, 1800 m and 2400 m elevation areas of the Pyrenees. ROS sensitivity to temperature  
552 and precipitation is evaluated by frequency, rainfall intensity and snow ablation during ROS days.

553 During the baseline climate period, annual ROS frequency totals on average 10, 12 and 10 day/season for 1500  
554 m, 1800 m and 2400 m elevations. Higher-than-average annual ROS frequency are found in 1800 m elevation  
555 SW (17 days/year) and NW (12 days/year), which contrast with the minimums detected in SE (9 days/year).  
556 The different spatial and seasonal ROS response to warming suggest that contrasting and shifting trends could  
557 be expected in the future. Overall ROS frequency decreases during summer in 2400 m elevation for > 1°C.  
558 When temperature is progressively increased the greatest ROS frequency increases are found for SW 2400 m  
559 elevation (around 1 day/month for + 1°C). ROS frequency is highly sensitive to warming in the snow onset  
560 and offset months, when counterintuitive factors play a key role. On the one hand, maximum Sf decreases are  
561 modeled for spring, leading to rainfall increases; on the other hand, warming depletes the snowpack in the  
562 warmest and snow driest sectors of the range. Consequently, data suggest a general ROS frequency decrease

for the majority of the SE massifs, where the snowpack is near the isothermal conditions in the baseline climate period. Yet, during spring, the highest ROS frequency increases are detected in SW and NW, since these sectors are less exposed to radiative and turbulent heat fluxes and record higher-than-average seasonal snow accumulations.

ROS rainfall amount generally increases due to warming, independently of the sector and elevation, being limited by the number of ROS days. The largest and constant increments are observed in spring, when ROS rainfall amount increases at a rate of 7, 6 and 3 % per °C for 1500 m, 1800 m and high, respectively. ROS rainfall amount increases are explained by Sf reductions, which decrease at a rate of 29 %, 22 %, and 12 % per °C for 1500 m, 1800 m, and 2400 m elevations, respectively. ROS rainfall amount maximum values are detected in SE (28 mm/day), especially in 1800 m elevation during autumn (45 mm/day), since this sector is exposed to subtropical Mediterranean flows.

Finally, ROS ablation shows contrasting patterns depending on the season, sector and elevation. Generally, ROS ablation increases in cold snowpacks, such as those modeled in 2400 m elevation and during cold seasons (autumn and winter). Here, ROS ablation follows a constant ablation rate of around + 10% per °C, due to higher-than-average positive sensible and LWin heat fluxes. However, in SE and 1500 m elevation, where marginal and isothermal snowpacks are found, no changes or decreases in ROS ablation are detected due to snowpack magnitude reductions in a warmer climate. Results demonstrate the high snow sensitivity to climate within a mid-latitude mountain range, and suggest significant changes with regards to water resources management. Relevant implications in the ecosystem and socio-economic activities associated with snow cover are anticipated.

### **Data availability**

FSM2 is an open access snow model (Essery, 2015) provided at <https://github.com/RichardEssery/FSM2> (last access 15 January 2023). SAFRAN climate dataset (Vernay et al., 2022) is available by AERIS at <https://www.aeris-data.fr/landing-page/?uuid=865730e8-cdeb-4c6b-ae58-80f95166509b#v2020.2> (last access 16 December 2022). Data of this work is available upon request by the first author ([josepbonsoms5@ub.edu](mailto:josepbonsoms5@ub.edu)).

### **Author contribution**

J.B., J.I.L.M., and E.A.G. designed the work. J.B. analyzed the data and wrote the manuscript. J.B., J.I.L.M., E.A.G., C.D.B., and M.O. provided feedback and edited the manuscript. J.I.L.M., M.O. supervised the project and acquired funding.

### **Competing interests**

The authors declare that they have no conflict of interest.

## 594 Acknowledgements

595 This work frames within the research topics examined by the research group “Antarctic, Arctic, Alpine  
596 Environments-ANTALP” (2017-SGR-1102) funded by the Government of Catalonia, HIDROIBERNIEVE  
597 (CGL2017-82216-R) and MARGISNOW (PID2021-124220OB-100), from the Spanish Ministry of Science,  
598 Innovation and Universities. JB is supported by a pre-doctoral University Professor FPI grant (PRE2021-  
599 097046) funded by the Spanish Ministry of Science, Innovation and Universities.

600

## 601 References

602

603 Alonso-González, E., Aalstad, K., Baba, M. W., Revuelto, J., López-Moreno, J. I., Fiddes, J., et al. MuSA: The  
604 Multiscale Snow Data Assimilation System (v1.0). *Geoscientific Model Development Discussions*, 1–43.  
605 <https://doi.org/10.5194/gmd-2022-137>, 2022.

606

607 Alonso-González, E., López-Moreno, J.I., Navarro-Serrano, F., Sanmiguel-Valladolid, A., Aznárez-Balta, M.,  
608 Revuelto, J., and Ceballos, A.: Snowpack Sensitivity to Temperature, Precipitation, and Solar Radiation  
609 Variability over an Elevational Gradient in the Iberian Mountains, *Atmos. Res.*, 243, 104973 <https://doi.org/10.1016/j.atmosres.2020.104973>, 2020a.

610

611  
612 Alonso-González, E., López-Moreno, J.I., Navarro-Serrano, F., Sanmiguel-Valladolid, A., Revuelto, J.,  
613 Domínguez-Castro, F., and Ceballos, A.: Snow climatology for the mountains in the Iberian Peninsula using  
614 satellite imagery and simulations with dynamically downscaled reanalysis data, *International Journal of*  
615 *Climatology*, 40(1), 477–491, <https://doi.org/10.1002/joc.6223>, 2019.

616

617 Alonso-González, E., López-Moreno, J. I., Navarro-Serrano, F. M., and Revuelto, J.: Impact of North Atlantic  
618 Oscillation on the snowpack in Iberian Peninsula mountains, *Water (Switzerland)*, 12,  
619 <https://doi.org/10.3390/w12010105>, 2020b.

620 Amblar-Francés, M. P., Ramos-Calzado, P., Sanchis-Lladó, J., Hernanz-Lázaro, A., Peral-García, M. C.,  
621 Navascués, B., Dominguez-Alonso, M., Pastor-Saavedra, M. A., and Rodríguez-Camino, E.: High resolution  
622 climate change projections for the Pyrenees region, in: *Advances in Science and Research*, 191–208,  
623 <https://doi.org/10.5194/asr-17-191-2020>, 2020.

624

625 Barnett, T.P., Adam, J.C., and Lettenmaier, D.P., Potential impacts of a warming climate on water availability  
626 in snow-dominated regions. *Nature*. <https://doi.org/10.1038/nature04141>, 2005.

627 Bartsch, A., Kumpula, T., Forbes, B. C., and Stammer, F.: Detection of snow surface thawing and refreezing  
628 in the Eurasian arctic with QuikSCAT: Implications for reindeer herding, *Ecological Applications*, 20, 2346–  
629 2358, <https://doi.org/10.1890/09-1927.1>, 2010.

630 Beniston, M. and Stoffel, M.: Rain-on-snow events, floods and climate change in the Alps: Events may increase  
631 with warming up to 4 °C and decrease thereafter, *Science of the Total Environment*, 571, 228–236,  
632 <https://doi.org/10.1016/j.scitotenv.2016.07.146>, 2016.

633 Beniston, M., Farinotti, D., Stoffel, M., Andreassen, L. M., Coppola, E., Eckert, N., Fantini, A., Giacona, F.,  
634 Hauck, C., Huss, M., Huwald, H., Lehning, M., López-Moreno, J. I., Magnusson, J., Marty, C., Morán-Tejeda,  
635 E., Morin, S., Naaim, M., Provenzale, A., Rabatel, A., Six, D., Stötter, J., Strasser, U., Terzago, S., and Vincent,  
636 C.: The European mountain cryosphere: A review of its current state, trends, and future challenges,  
637 <https://doi.org/10.5194/tc-12-759-2018>, 2018.

638 Bieniek, P. A., Bhatt, U. S., Walsh, J. E., Lader, R., Griffith, B., Roach, J. K., and Thoman, R. L.: Assessment  
639 of Alaska rain-on-snow events using dynamical downscaling, *J Appl Meteorol Climatol*, 57, 1847–1863,  
640 <https://doi.org/10.1175/JAMC-D-17-0276.1>, 2018.

641 Bintanja, R. and Andry, O.: Towards a rain-dominated Arctic, *Nat Clim Chang*, 7, 263–267,  
642 <https://doi.org/10.1038/nclimate3240>, 2017.

643 Bonsoms, J., Franch, F. S., and Oliva, M.: Snowfall and snow cover evolution in the eastern pre-pyrenees (Ne  
644 iberian peninsula), *Geographical Research Letters*, 47, 291–307, <https://doi.org/10.18172/cig.4879>, 2021a.

645 Bonsoms, J., González, S., Prohom, M., Esteban, P., Salvador-Franch, F., López-Moreno, J. I., and Oliva, M.:  
646 Spatio-temporal patterns of snow in the Catalan Pyrenees (NE Iberia), *International Journal of Climatology*,  
647 41, 5676–5697, <https://doi.org/10.1002/joc.7147>, 2021b.

648 Bonsoms, J., López-Moreno, J. I., González, S., and Oliva, M.: Increase of the energy available for snow  
649 ablation in the Pyrenees (1959–2020) and its relation to atmospheric circulation, *Atmos Res*, 275,  
650 <https://doi.org/10.1016/j.atmosres.2022.106228>, 2022a.

651 Bonsoms, J., López-Moreno, J. I., and Alonso-González, E.: Snow sensitivity to temperature and precipitation  
652 change during compound cold–hot and wet–dry seasons in the Pyrenees, *The Cryosphere*, 17, 1307–1326,  
653 <https://doi.org/10.5194/tc-17-1307-2023>, 2023.

654 Buisan, S.T., López-Moreno, J.I., Sanz, M.A. and Korchendorfer, J. Impact of weather type variability on  
655 winter precipitation, temperature and annual snowpack in the Spanish Pyrenees. *Climate Research*, 69, 79–92.  
656 <https://doi.org/10.3354/cr01391>, 2016.

657 Bjerke JW, Treharne R, Vikhamar-Schuler D, Karlsen S R, Ravolainen V, Bokhorst S, Phoenix G K, Bochenek  
658 Z and Tømmervik H 2017 Understanding the drivers of extensive plant damage in boreal and Arctic  
659 ecosystems: insights from field surveys in the aftermath of damage *Sci. Total Environ.* 599 1965–76.

660 Ceron, J. P., Tanguy, G., Franchistéguy, L., Martin, E., Regimbeau, F., and Vidal, J. P.: Hydrological seasonal  
661 forecast over France: Feasibility and prospects, *Atmospheric Science Letters*, 11, 78–82,  
662 <https://doi.org/10.1002/asl.256>, 2010.

663 Cohen, J., Ye, H., and Jones, J.: Trends and variability in rain-on-snow events, *Geophys Res Lett*, 42, 7115–  
664 7122, <https://doi.org/10.1002/2015GL065320>, 2015.

665 Collados-Lara, A. J., Pulido-Velazquez, D., Pardo-Igúzquiza, E., and Alonso-González, E.: Estimation of the  
666 spatio-temporal dynamic of snow water equivalent at mountain range scale under data scarcity, *Science of the*  
667 *Total Environment*, 741, <https://doi.org/10.1016/j.scitotenv.2020.140485>, 2020.

668 Conway, H. and Raymond, C. F.: Snow stability during rain, *Journal of Glaciology*, 39, 635–642,  
669 <https://doi.org/10.3189/s0022143000016531>, 1993.

670 Corripio, J. G. and López-Moreno, J. I.: Analysis and predictability of the hydrological response of mountain  
671 catchments to heavy rain on snow events: A case study in the Spanish Pyrenees, *Hydrology*, 4,  
672 <https://doi.org/10.3390/hydrology4020020>, 2017.

673 Crawford, A. D., Alley, K. E., Cooke, A. M., and Serreze, M. C.: Synoptic Climatology of Rain-on-Snow  
674 Events in Alaska, <https://doi.org/10.1175/MWR-D-19>, 2020.

675 Deschamps-Berger, C., Cluzet, B., Dumont, M., Lafaysse, M., Berthier, E., Fanise, P., and Gascoin, S.:  
676 Improving the Spatial Distribution of Snow Cover Simulations by Assimilation of Satellite Stereoscopic



677 Imagery, *Water Resour. Res.*, 58, e2021WR030271, <https://doi.org/10.1029/2021WR030271>, 2022.

678

679 Del Barrio, G., Creus, J., and Puigdefabregas, J.: Thermal Seasonality of the High Mountain Belts of the

680 Pyrenees, *Mt. Res. Dev.*, 10, 227–233, 1990.

681 Devers, A., Vidal, J. P., Lauvernet, C., and Vannier, O.: FYRE Climate: A high-resolution reanalysis of daily

682 precipitation and temperature in France from 1871 to 2012, *Climate of the Past*, 17, 1857–1879,

683 <https://doi.org/10.5194/cp-17-1857-2021>, 2021.

684 Durand, Y., Giraud, G., Brun, E., Mérindol, L., and Martin, E.: A computer-based system simulating snowpack

685 structures as a tool for regional avalanche forecasting, *Journal of Glaciology*, 45, 469–484,

686 <https://doi.org/10.3189/s0022143000001337>, 1999.

687 Durand, Y., Laternser, M., Giraud, G., Etchevers, P., Lesaffre, B., and Mérindol, L.: Reanalysis of 44 yr of

688 climate in the French Alps (1958–2002): Methodology, model validation, climatology, and trends for air

689 temperature and precipitation, *J Appl Meteorol Climatol*, 48, 429–449,

690 <https://doi.org/10.1175/2008JAMC1808.1>, 2009.

691 Essery, R.: A factorial snowpack model (FSM 1.0), *Geosci Model Dev*, 8, 3867–3876,

692 <https://doi.org/10.5194/gmd-8-3867-2015>, 2015.

693

694 Essery, R., Kim, H., Wang, L., Bartlett, P., Boone, A., Brutel-Vuilmet, C., Burke, E., Cuntz, M., Decharme,

695 B., Dutra, E., Fang, X., Gusev, Y., Hagemann, S., Haverd, V., Kontu, A., Krinner, G., Lafaysse, M., Lejeune,

696 Y., Marke, T., Marks, D., Marty, C., Menard, C. B., Nasonova, O., Nitta, T., Pomeroy, J., Schädler, G.,

697 Semenov, V., Smirnova, T., Swenson, S., Turkov, D., Wever, N., and Yuan, H.: Snow cover duration trends

698 observed at sites and predicted by multiple models, *Cryosphere*, 14, 4687–4698, [https://doi.org/10.5194/tc-](https://doi.org/10.5194/tc-14-4687-2020)

699 14-4687-2020, 2020.

700 Freudiger, D., Kohn, I., Stahl, K., and Weiler, M.: Large-scale analysis of changing frequencies of rain-on-

701 snow events with flood-generation potential, *Hydrol Earth Syst Sci*, 18, 2695–2709,

702 <https://doi.org/10.5194/hess-18-2695-2014>, 2014.

703 García-Ruiz, J. M., López-Moreno, J. I., Vicente-Serrano, S. M., Lasanta-Martínez, T. and Beguería, S.

704 Mediterranean water resources in a global change scenario, *Earth Sci. Rev.*, 105(3–4), 121–139,

705 <https://doi.org/10.1016/j.earscirev.2011.01.006>, 2011.

706 Garvelmann, J., Pohl, S., and Weiler, M.: Variability of observed energy fluxes during rain-on-snow and clear

707 sky snowmelt in a midlatitude mountain environment, *J Hydrometeorol*, 15, 1220–1237,

708 <https://doi.org/10.1175/JHM-D-13-0187.1>, 2014.

709 Günther, D., Marke, T., Essery, R., and Strasser, U.: Uncertainties in Snowpack Simulations—Assessing the

710 Impact of Model Structure, Parameter Choice, and Forcing Data Error on Point-Scale Energy Balance Snow

711 Model Performance, *Water Resour Res*, 55, 2779–2800, <https://doi.org/10.1029/2018WR023403>, 2019.

712 Habets, F., Boone, A., Champeaux, J. L., Etchevers, P., Franchistéguy, L., Leblois, E., Ledoux, E., le Moigne,

713 P., Martin, E., Morel, S., Noilhan, J., Seguí, P. Q., Rousset-Regimbeau, F., and Viennot, P.: The SAFRAN-

714 ISBA-MODCOU hydrometeorological model applied over France, *Journal of Geophysical Research*

715 *Atmospheres*, 113, <https://doi.org/10.1029/2007JD008548>, 2008.

716 Hansen, B.B., Grøtan, V., Aanes, R., et al., 2013. Climate events synchronize the dynamics of a resident

717 vertebrate community in the High Arctic. *Science* 339, 313–315.

- 718 Hansen, B.B., Isaksen, K., Benestad, R.E., et al., 2014. Warmer and wetter winters: characteristics and  
719 implications of an extreme weather event in the High Arctic. *Environ. Res. Lett.* 9, 114021. Harder, P. and  
720 Pomeroy, J.: Estimating precipitation phase using a psychrometric energy balance method, *Hydrological*  
721 *Processes*, 27(13), 1901–1914. <https://doi.org/10.1002/hyp.9799>, 2013
- 722 Immerzeel, W. W., Lutz, A. F., Andrade, M., Bahl, A., Biemans, H., Bolch, T., Hyde, S., Brumby, S., Davies,  
723 B. J., Elmore, A. C., Emmer, A., Feng, M., Fernández, A., Haritashya, U., Kargel, J. S., Koppes, M.,  
724 Kraaijenbrink, P. D. A., Kulkarni, A. v., Mayewski, P. A., Nepal, S., Pacheco, P., Painter, T. H., Pellicciotti, F.,  
725 Rajaram, H., Rupper, S., Sinisalo, A., Shrestha, A. B., Viviroli, D., Wada, Y., Xiao, C., Yao, T., and Baillie, J.  
726 E. M.: Importance and vulnerability of the world's water towers, *Nature*, 577, 364–369,  
727 <https://doi.org/10.1038/s41586-019-1822-y>, 2020.
- 728 IPCC: High Mountain Areas, in: *The Ocean and Cryosphere in a Changing Climate*, Cambridge University  
729 Press, 131–202, <https://doi.org/10.1017/9781009157964.004>, 2022.
- 730 Jennings, K. S., Winchell, T. S., Livneh, B., and Molotch, N. P.: Spatial variation of the rain-snow temperature  
731 threshold across the Northern Hemisphere, *Nat Commun*, 9, <https://doi.org/10.1038/s41467-018-03629-7>,  
732 2018.
- 733 il Jeong, D. and Sushama, L.: Rain-on-snow events over North America based on two Canadian regional  
734 climate models, *Clim Dyn*, 50, 303–316, <https://doi.org/10.1007/s00382-017-3609-x>, 2018.
- 735 Kohler, J. and Aanes, R.: Effect of winter snow and ground-icing on a Svalbard reindeer population: Results  
736 of a simple snowpack model, in: *Arctic, Antarctic, and Alpine Research*, 333–341,  
737 [https://doi.org/10.1657/1523-0430\(2004\)036\[0333:EOWSAG\]2.0.CO;2](https://doi.org/10.1657/1523-0430(2004)036[0333:EOWSAG]2.0.CO;2), 2004.
- 738 Krinner, G., Derksen, C., Essery, R., Flanner, M., Hagemann, S., Clark, M., Hall, A., Rott, H., Brutel-  
739 Vuilmet, C., Kim, H., Ménard, C. B., Mudryk, L., Thackeray, C., Wang, L., Arduini, G., Balsamo, G.,  
740 Bartlett, P., Boike, J., Boone, A., Chéruy, F., Colin, J., Cuntz, M., Dai, Y., Decharme, B., Derry, J.,  
741 Ducharne, A., Dutra, E., Fang, X., Fierz, C., Ghattas, J., Gusev, Y., Haverd, V., Kontu, A., Lafaysse, M.,  
742 Law, R., Lawrence, D., Li, W., Marke, T., Marks, D., Ménégoz, M., Nasonova, O., Nitta, T., Niwano, M.,  
743 Pomeroy, J., Raleigh, M. S., Schaedler, G., Semenov, V., Smirnova, T. G., Stacke, T., Strasser, U.,  
744 Svenson, S., Turkov, D., Wang, T., Wever, N., Yuan, H., Zhou, W., and Zhu, D.: ESM-SnowMIP: assessing  
745 snow models and quantifying snow-related climate feedbacks, *Geosci. Model Dev.*, 11, 5027–5049,  
746 <https://doi.org/10.5194/gmd-11-5027-2018>, 2018.
- 747 Lemus-Canovas, M., Lopez-Bustins, J. A., Trapero, L., and Martin-Vide, J.: Combining circulation weather  
748 types and daily precipitation modelling to derive climatic precipitation regions in the Pyrenees, *Atmos Res*,  
749 220, 181–193, <https://doi.org/10.1016/j.atmosres.2019.01.018>, 2019.
- 750 Lemus-Canovas, M., Lopez-Bustins, J. A., Martín-Vide, J., Halifa-Marin, A., Insua-Costa, D., Martinez-  
751 Artigas, J., Trapero, L., Serrano-Notivol, R., and Cuadrat, J. M.: Characterisation of extreme precipitation  
752 events in the Pyrenees: From the local to the synoptic scale, *Atmosphere (Basel)*, 12,  
753 <https://doi.org/10.3390/atmos12060665>, 2021.
- 754 Li, D., Lettenmaier, D. P., Margulis, S. A., and Andreadis, K.: The Role of Rain-on-Snow in Flooding Over  
755 the Conterminous United States, *Water Resour Res*, 55, 8492–8513, <https://doi.org/10.1029/2019WR024950>,  
756 2019.
- 757 Llasat, M. C., Marcos, R., Llasat-Botija, M., Gilabert, J., Turco, M., and Quintana-Seguí, P.: Flash flood  
758 evolution in North-Western Mediterranean, *Atmos Res*, 149, 230–243,

759 <https://doi.org/10.1016/j.atmosres.2014.05.024>, 2014. López-Moreno, J. I.: Recent variations of snowpack  
 760 depth in the central Spanish Pyrenees, *Arct Antarct Alp Res*, 37, 253–260, [https://doi.org/10.1657/1523-0430\(2005\)037\[0253:RVOSDI\]2.0.CO;2](https://doi.org/10.1657/1523-0430(2005)037[0253:RVOSDI]2.0.CO;2), 2005.

762 López-Moreno, J.I., Goyette, S., and Beniston, M.: Climate change prediction over complex areas: spatial  
 763 variability of uncertainties and predictions over the Pyrenees from a set of regional climate models.  
 764 *International Journal of Climatology*, 28, 1535–1550. <https://doi.org/10.1002/joc.1645>, 2008.

765 López-Moreno, J. I., Pomeroy, J. W., Revuelto, J., and Vicente-Serrano, S. M.: Response of snow processes to  
 766 climate change: Spatial variability in a small basin in the Spanish Pyrenees, *Hydrol Process*, 27, 2637–2650,  
 767 <https://doi.org/10.1002/hyp.9408>, 2013.

768 López-Moreno, J. I., Pomeroy, J. W., Morán-Tejeda, E., Revuelto, J., Navarro-Serrano, F. M., Vidaller, I., and  
 769 Alonso-González, E.: Changes in the frequency of global high mountain rain-on-snow events due to climate  
 770 warming, *Environmental Research Letters*, 16, <https://doi.org/10.1088/1748-9326/ac0dde>, 2021.

771 López-Moreno, J.I., Soubeyroux, J.M., Gascoin, S., Alonso-González, E., Durán-Gómez, N., Lafaysse, M.,  
 772 Vernay, M., Carmagnola, C. and Morin, S. Long-term trends (1958–2017) in snow cover duration and depth  
 773 in the Pyrenees. *International Journal of Climatology*, 40, 1–15. <https://doi.org/10.1002/joc.6571>, 2020.

774 López-Moreno, J.I., and Vicente-Serrano, S.M.: Atmospheric circulation influence on the interannual  
 775 variability of snowpack in the Spanish Pyrenees during the second half of the twentieth century, *Nord. Hydrol.*,  
 776 38 (1), 38–44, <https://doi.org/10.2166/nh.2007.030>, 2007.

777 López-Moreno, J.I., and Latron, J., 2008. Spatial heterogeneity in snow water equivalent induced by forest  
 778 canopy in a mixed beech-fir stand in the Pyrenees. *Ann. Glaciol.* 49 (1), 83–90,  
 779 <https://doi.org/10.3189/172756408787814951>, 2008.

780 Loukas, A., Vasiliades, L., and Dalezios, N. R.: Potential climate change impacts on flood producing  
 781 mechanisms in southern British Columbia, Canada using the CGCMA1 simulation results, *J. Hydrol.*, 259,  
 782 163–188, [https://doi.org/10.1016/S0022-1694\(01\)00580-7](https://doi.org/10.1016/S0022-1694(01)00580-7), 2002

783 Lundquist, J. D., Dickerson-Lange, S. E., Lutz, J. A., and Cristea, N. C.: Lower forest density enhances snow  
 784 retention in regions with warmer winters: A global framework developed from plot-scale observations and  
 785 modeling, *Water Resour Res*, 49, 6356–6370, <https://doi.org/10.1002/wrcr.20504>, 2013.

786 Lynn, E., Cuthbertson, A., He, M., Vasquez, J. P., Anderson, M. L., Coombe, P., Abatzoglou, J. T., and Hatchett,  
 787 B. J.: Technical note: Precipitation-phase partitioning at landscape scales to regional scales, *Hydrol Earth Syst*  
 788 *Sci*, 24, 5317–5328, <https://doi.org/10.5194/hess-24-5317-2020>, 2020.

789 Matiu, M., Crespi, A., Bertoldi, G., Carmagnola, C.M., Marty, C., Morin, S., Schöner, W., Cat Berro, D.,  
 790 Chiogna, G., De Gregorio, L., Kotlarski, S., Majone, B., Resch, G., Terzago, S., Valt, M., Beozzo, W.,  
 791 Cianfarra, P., Gouttevin, I., Marcolini, G., Notarnicola, C., Petitta, M., Scherrer, S.C., Strasser, U., Winkler,  
 792 M., Zebisch, M., Cicogna, A., Cremonini, R., Debernardi, A., Faletto, M., Gaddo, M., Giovannini, L., Mercalli,  
 793 L., Soubeyroux, J.-M., Susnik, A., Trenti, A., Urbani, S., Weigluni, V. Observed snow depth trends in the  
 794 European Alps 1971 to 2019. *Cryosphere*, 1–50. <https://doi.org/10.5194/tc-2020-289>, 2020.

795 Marks, D., Link, T., Winstral, A., and Garen, D.: Simulating snowmelt processes during rain-on-snow over a  
 796 semi-arid mountain basin, 1992.

797 Marty, C., Schlögl, S., Bavay, M., and Lehning, M.: How much can we save? Impact of different emission

798 scenarios on future snow cover in the Alps, *Cryosphere*, 11, 517–529, <https://doi.org/10.5194/tc-11-517-2017>,  
799 2017.

800 Mazurkiewicz, A. B., Callery, D. G., and McDonnell, J. J.: Assessing the controls of the snow energy balance  
801 and water available for runoff in a rain-on-snow environment, *J Hydrol (Amst)*, 354, 1–14,  
802 <https://doi.org/10.1016/j.jhydrol.2007.12.027>, 2008.

803 Mazzotti, G., Essery, R., Webster, C., Malle, J., and Jonas, T.: Process-Level Evaluation of a Hyper-Resolution  
804 Forest Snow Model Using Distributed Multisensor Observations, *Water Resour Res*, 56,  
805 <https://doi.org/10.1029/2020WR027572>, 2020.

806 McCabe, G. J., Clark, M. P., and Hay, L. E.: Rain-on-snow events in the Western United-States,  
807 <https://doi.org/10.1175/BAMS-88-3-319>, 2007.

808 Mooney, P. A. and Li, L.: Near future changes to rain-on-snow events in Norway, *Environmental Research*  
809 *Letters*, 16, <https://doi.org/10.1088/1748-9326/abfdeb>, 2021.

810 Morán-Tejeda, E., López-Moreno, J. I., Stoffel, M., and Beniston, M.: Rain-on-snow events in Switzerland:  
811 Recent observations and projections for the 21st century, *Clim Res*, 71, 111–125,  
812 <https://doi.org/10.3354/cr01435>, 2016.

813 Morán-Tejeda, E., Fassnacht, S. R., Lorenzo-Lacruz, J., López-Moreno, J. I., García, C., Alonso-González, E.,  
814 and Collados-Lara, A. J.: Hydro-meteorological characterization of major floods in Spanish mountain rivers,  
815 *Water (Switzerland)*, 11, <https://doi.org/10.3390/W11122641>, 2019.

816 Morin, S., Horton, S., Techel, F., Bavay, M., Coléou, C., Fierz, C., Gobiet, A., Hagenmuller, P., Lafaysse, M.,  
817 Ližar, M., Mitterer, C., Monti, F., Müller, K., Olefs, M., Snook, J. S., van Herwijnen, A., and Vionnet, V.:  
818 Application of physical snowpack models in support of operational avalanche hazard forecasting: A status  
819 report on current implementations and prospects for the future,  
820 <https://doi.org/10.1016/j.coldregions.2019.102910>, 2020.

821 Musselman, K. N., Clark, M. P., Liu, C., Ikeda, K., and Rasmussen, R.: Slower snowmelt in a warmer world,  
822 *Nat Clim Chang*, 7, 214–219, <https://doi.org/10.1038/nclimate3225>, 2017a.

823 Musselman, K. N., Keitholotch, N. P., Mar, N., and Mgulis, S. A.: Snowmelt response to simulated warming  
824 across a large elevation gradient, southern sierra Nevada, California, *Cryosphere*, 11, 2847–2866,  
825 <https://doi.org/10.5194/tc-11-2847-2017>, 2017b.

826 Musselman, K. N., Lehner, F., Ikeda, K., Clark, M. P., Prein, A. F., Liu, C., Barlage, M., and Rasmussen, R.:  
827 Projected increases and shifts in rain-on-snow flood risk over western North America,  
828 <https://doi.org/10.1038/s41558-018-0236-4>, 2018.

829 Navarro-Serrano, F. and López-Moreno, J. I.: Análisis espacio-temporal de los eventos de nevadas en el pirineo  
830 Español y su relación con la circulación atmosférica, *Cuadernos de Investigacion Geografica*, 43, 233–254,  
831 <https://doi.org/10.18172/cig.3042>, 2017.

832 Ohba, M. and Kawase, H.: Rain-on-Snow events in Japan as projected by a large ensemble of regional climate  
833 simulations, *Clim Dyn*, 55, 2785–2800, <https://doi.org/10.1007/s00382-020-05419-8>, 2020.

834

835 OPCC-CTP. Climate change in the Pyrenees: Impacts, vulnerabilities and adaptation bases of knowledge for  
836 the future climate change adaptation strategy in the Pyrenees. 2018. 147. Jaca, Spain.

837 [https://www.opccctp.org/sites/default/files/editor/ opcc-informe-en-paginas.pdf](https://www.opccctp.org/sites/default/files/editor/opcc-informe-en-paginas.pdf). (last acces December 25,  
838 2022)

839 Pall, P., Tallaksen, L. M., and Stordal, F.: A Climatology of Rain-on-Snow Events for Norway,  
840 <https://doi.org/10.1175/JCLI-D-18, 2019>.

841 Pepin, N. C., Arnone, E., Gobiet, A., Haslinger, K., Kotlarski, S., Notarnicola, C., Palazzi, E., Seibert, P.,  
842 Serafin, S., Schöner, W., Terzago, S., Thornton, J. M., Vuille, M., and Adler, C.: Climate Changes and Their  
843 Elevational Patterns in the Mountains of the World, <https://doi.org/10.1029/2020RG000730>, 2022.

844 Peña-Angulo, D., Vicente-Serrano, S., Domínguez-Castro, F., Murphy, C., Reig, F., Trambay, Y., Trigo, R.,  
845 Luna, M.Y., Turco, M., Noguera, I., Aznarez-Balta, M., Garcia-Herrera, R., Tomas-Burguera, M. and Kenawy,  
846 A. Long-term precipitation in Southwestern Europe reveals no clear trend attributable to anthropogenic  
847 forcing. *Environmental Research Letters*, 15, 094070 <https://doi.org/10.1088/1748-9326/ab9c4f>, 2020.

848 Pons, M., López-Moreno, J., Rosas-Casals, M., and Jover, E.: The vulnerability of Pyrenean ski resorts to  
849 climate-induced changes in the snowpack, *Clim. Change*, 131, 591–605, [https://doi.org/10.1007/s10584-015-](https://doi.org/10.1007/s10584-015-1400-8)  
850 [1400-8](https://doi.org/10.1007/s10584-015-1400-8), 2015.

851 Pomeroy, J. W., Fang, X., and Rasouli, K.: Sensitivity of snow processes to warming in the Canadian Rockies,  
852 2015.

853 Pomeroy, J. W., Fang, X., and Marks, D. G.: The cold rain-on-snow event of June 2013 in the Canadian Rockies  
854 — characteristics and diagnosis, *Hydrol Process*, 30, 2899–2914, <https://doi.org/10.1002/hyp.10905>, 2016.

855 Rasouli, K., Pomeroy, J. W., and Whitfield, P. H.: Hydrological responses of headwater basins to monthly  
856 perturbed climate in the North American Cordillera, *J Hydrometeorol*, 20, 863–882,  
857 <https://doi.org/10.1175/JHM-D-18-0166.1>, 2019.

858 Rennert, K. J., Roe, G., Putkonen, J., and Bitz, C. M.: Soil thermal and ecological impacts of rain on snow  
859 events in the circumpolar arctic, *J Clim*, 22, 2302–2315, <https://doi.org/10.1175/2008JCLI2117.1>, 2009.

860 Réveillet, M., Dumont, M., Gascoin, S., Lafaysse, M., Nabat, P., Ribes, A., Nheili, R., Tuzet, F., Ménégoz, M.,  
861 Morin, S., Picard, G., and Ginoux, P.: Black carbon and dust alter the response of mountain snow cover under  
862 climate change, *Nat Commun*, 13, <https://doi.org/10.1038/s41467-022-32501-y>, 2022.

863 Revuelto, J., Lecourt, G., Lafaysse, M., Zin, I., Charrois, L., Vionnet, V., Dumont, M., Rabatel, A., Six, D.,  
864 Condom, T., Morin, S., Viani, A., and Sirguey, P.: Multi-criteria evaluation of snowpack simulations in  
865 complex alpine terrain using satellite and in situ observations, *Remote Sens (Basel)*, 10,  
866 <https://doi.org/10.3390/rs10081171>, 2018.

867 Roe, G. H. and Baker, M. B.: *Microphysical and Geometrical Controls on the Pattern of Orographic*  
868 *Precipitation*, 2006.

869 Sanmiguel-Valladolid, A., McPhee, J., Esmeralda Ojeda Carreño, P., Morán-Tejeda, E., Julio Camarero, J., and  
870 López-Moreno, J. I.: Sensitivity of forest–snow interactions to climate forcing: Local variability in a Pyrenean  
871 valley, *J Hydrol (Amst)*, 605, <https://doi.org/10.1016/j.jhydrol.2021.127311>, 2022.

872

873 Schirmer, M., Winstral, A., Jonas, T., Burlando, P., and Peleg, N.: Natural climate variability is an important  
874 aspect of future projections of snow water resources and rain-on-snow events, *Cryosphere*, 16, 3469–3488,  
875 <https://doi.org/10.5194/tc-16-3469-2022>, 2022.

- 876 Schöner, W., Koch, R., Matulla, C., Marty, C., and Tilg, A. M.: Spatio-temporal patterns of snow depth within  
877 the Swiss-Austrian Alps for the past half century (1961 to 2012) and linkages to climate change, *International*  
878 *Journal of Climatology*, 39, 1589–1603, <https://doi.org/10.1002/joc.5902>, 2019.
- 879 Serrano-Notivoli, R., Buisan, S.T., Abad-Pérez, L.M., Sierra-Álvarez, E., Rodríguez-Ballesteros, C., López-  
880 Moreno, J.I. and Cuadrat, J.M. Tendencias recientes en precipitación, temperatura y nieve de alta montaña en  
881 los Pirineos (Refugio de Góriz, Huesca). In: *El clima: aire, agua, tierra y fuego*. Madrid, Spain: Asociación  
882 Española de Climatología y Ministerio para la Transición Ecológica – Agencia Estatal de Meteorología, pp.  
883 267, 1060–280, 2018.
- 884 Serrano-Notivoli, R., Mora, D., Ollero, A., Sánchez-Fabre, M., Sanz, P., and Saz, M.: Floodplain occupation  
885 and flooding in the central Pyrenees, *Cuadernos de Investigacion Geografica*, 43, 309–328,  
886 <https://doi.org/10.18172/cig.3057>, 2017.
- 887 Serreze, M. C., Gustafson, J., Barrett, A. P., Druckenmiller, M. L., Fox, S., Voveris, J., Stroeve, J., Sheffield,  
888 B., Forbes, B. C., Rasmus, S., Laptander, R., Brook, M., Brubaker, M., Temte, J., McCrystall, M. R., and  
889 Bartsch, A.: Arctic rain on snow events: Bridging observations to understand environmental and livelihood  
890 impacts, *Environmental Research Letters*, 16, <https://doi.org/10.1088/1748-9326/ac269b>, 2021.
- 891 Shanley, J. B. and Chalmers, A.: The effect of frozen soil on snowmelt runoff at Sleepers River, Vermont 1999.
- 892 Singh, P., Spitzbart, G., Hübl, H., and Weinmeister, H. W.: Hydrological response of snowpack under rain-on-  
893 snow events: a field study, *Journal of Hydrology*, 1–20 pp., 1997.
- 894 Smyth, E. J., Raleigh, M. S., and Small, E. E. (2020). Improving SWE estimation with data assimilation: The  
895 influence of snow depth observation timing and uncertainty. *Water Resources Research*, 56, e2019WR026853.  
896 <https://doi.org/10.1029/2019WR026853>
- 897 Spandre, P., François, H., Verfaillie, D., Lafaysse, M., Déqué, M., Eckert, N., George, E., and Morin, S.:  
898 Climate controls on snow reliability in French Alps ski resorts, *Sci Rep*, 9, [https://doi.org/10.1038/s41598-](https://doi.org/10.1038/s41598-019-44068-8)  
899 019-44068-8, 2019.
- 900 Stewart, I. T.: Changes in snowpack and snowmelt runoff for key mountain regions,  
901 <https://doi.org/10.1002/hyp.7128>, 2009.
- 902 Surfleet, C. G. and Tullos, D.: Variability in effect of climate change on rain-on-snow peak flow events in a  
903 temperate climate, *J Hydrol (Amst)*, 479, 24–34, <https://doi.org/10.1016/j.jhydrol.2012.11.021>, 2013.
- 904 Szczypta, C., Gascoin, S., Houet, T., Hagolle, O., Dejoux, J.-F., Vigneau, C., and Fanise, P.: Impact of climate  
905 and land cover changes on snow cover in a small Pyrenean catchment, *J. Hydrol.*, 521, 84–99,  
906 [doi:10.1016/j.jhydrol.2014.11.060](https://doi.org/10.1016/j.jhydrol.2014.11.060), 2015.
- 907 Verfaillie, D., Lafaysse, M., Déqué, M., Eckert, N., Lejeune, Y., and Morin, S.: Multi-component ensembles  
908 of future meteorological and natural snow conditions for 1500 m altitude in the Chartreuse mountain range,  
909 *Northern French Alps, Cryosphere*, 12, 1249–1271, <https://doi.org/10.5194/tc-12-1249-2018>, 2018.
- 910 Vernay, M., Lafaysse, M., Monteiro, D., Hagenmuller, P., Nheili, R., Samacoïts, R., Verfaillie, D., and Morin,  
911 S.: The S2M meteorological and snow cover reanalysis over the French mountainous areas: description and  
912 evaluation (1958-2021), *Earth Syst Sci Data*, 14, 1707–1733, <https://doi.org/10.5194/essd-14-1707-2022>,  
913 2022.
- 914 Vicente-Serrano, S.M., Rodríguez-Camino, E., Domínguez-Castro, F., El Kenawy, A., Azorín-Molina, C. An

915 updated review on recent trends in observational surface atmospheric variables and their extremes over Spain.  
 916 Cuadernos de Investigación Geográfica (Geographical Research Letters) 43 (1), 209-232.  
 917 <https://doi.org/10.18172/cig.3134>, 2017.

918 Vidaller, I., Revuelto, J., Izagirre, E., Rojas-Heredia, F., Alonso-González, E., Gascoin, S., René, P., Berthier,  
 919 E., Rico, I., Moreno, A., Serrano, E., Serreta, A., López-Moreno, J.I. Toward an ice-free mountain range:  
 920 Demise of Pyrenean glaciers during 2011–2020. J. Geophys. Res. Lett. 48, e2021GL094339  
 921 <https://doi.org/10.1029/2021GL094339>, 2021.

922 Viviroli, D., Archer, D. R., Buytaert, W., Fowler, H. J., Greenwood, G. B., Hamlet, A. F., Huang, Y.,  
 923 Koboltschnig, G., Litaor, M. I., López-Moreno, J. I., Lorentz, S., Schädler, B., Schreier, H., Schwaiger, K.,  
 924 Vuille, M., and Woods, R.: Climate change and mountain water resources: Overview and recommendations  
 925 for research, management and policy, Hydrol Earth Syst Sci, 15, 471–504, [https://doi.org/10.5194/hess-15-](https://doi.org/10.5194/hess-15-471-2011)  
 926 471-2011, 2011.

927 Westermann, S., Boike, J., Langer, M., Schuler, T. V., and Etzelmüller, B.: Modeling the impact of wintertime  
 928 rain events on the thermal regime of permafrost, Cryosphere, 5, 945–959, [https://doi.org/10.5194/tc-5-945-](https://doi.org/10.5194/tc-5-945-2011)  
 929 2011, 2011.

930 Wipf, S. and Rixen, C.: A review of snow manipulation experiments in Arctic and alpine tundra ecosystems,  
 931 <https://doi.org/10.1111/j.1751-8369.2010.00153.x>, 2010.

932 Wu, X., Che, T., Li, X., Wang, N., and Yang, X.: Slower Snowmelt in Spring Along With Climate Warming  
 933 Across the Northern Hemisphere, Geophys Res Lett, 45, 12,331-12,339,  
 934 <https://doi.org/10.1029/2018GL079511>, 2018.

935 Würzer, S., Jonas, T., Wever, N., and Lehning, M.: Influence of initial snowpack properties on runoff formation  
 936 during rain-on-snow events, J Hydrometeorol, 17, 1801–1815, <https://doi.org/10.1175/JHM-D-15-0181.1>,  
 937 2016.

938